Eukaryotic translation initiation factor eIF4E-5 is required for spermiogenesis in *Drosophila melanogaster*

Lisa Shao[1,2], Jaclyn M. Fingerhut[3], Brook L. Falk[1,2], Hong Han[4], Giovanna Maldonado[5], Yuemeng Qiao[1,6], Vincent Lee[1,2,7], Elizabeth Hall[1,2,8], Liang Chen[4,9], Gordon Polevoy[1], Greco Hernández[5], Paul Lasko[4], Julie A. Brill[1,2,*]

[1]Cell Biology Program, The Hospital for Sick Children, PGCRL Building, 686 Bay Street, Toronto, Ontario, M5G 0A4, Canada
[2]Department of Molecular Genetics, University of Toronto, 1 King's College Circle, Toronto, Ontario, M5S 1A8, Canada
[3]Whitehead Institute for Biomedical Research, 455 Main St, Cambridge, Massachusetts, MA 02142, USA; and Howard Hughes Medical Institute
[4]Department of Biology, McGill University, 3649 Promenade Sir William Osler, Montréal, Quebec, H3G 0B1, Canada
[5]Laboratory of Translation and Cancer, Unit of Biomedical Research on Cancer, Instituto Nacional de Cancerología (INCan), Av San Fernando 22, Mexico City, 14080, Mexico
[6]Human Biology Program, University of Toronto, 300 Huron Street, Toronto, Ontario, M5S 3J6, Canada
[7]Present address: Clarivate Analytics, 150 King St. W, Toronto, Ontario, M5H 1J9, Canada
[8]Present address: Faculty of Medicine, University of Toronto, 1 King's College Circle, Toronto, Ontario, M5S 1A8, Canada
[9]Present address: Internal Medicine, Montreal General Hospital, 1650 Cedar Ave., Montreal, QC, H3G 1A4

[*]To whom correspondence should be addressed:
Julie A. Brill <julie.brill@sickkids.ca>

Keywords: post-transcriptional regulation, eIF4E variant, spermatogenesis, individualization, spermatid cyst polarity, male fertility

Summary Statement

The testis-enriched translation initiation factor eIF4E-5 contributes to spermatid cyst polarization and is needed for individualization of mature sperm and male fertility in *Drosophila*.

Abstract

Drosophila sperm development is characterized by extensive post-transcriptional regulation whereby thousands of transcripts are preserved for translation during later stages. A key step in translation initiation is the binding of eukaryotic initiation factor 4E (eIF4E) to the 5' mRNA cap. In addition to canonical eIF4E-1, *Drosophila* has multiple eIF4E paralogs, including four (eIF4E-3, -4, -5, and -7) that are highly expressed in the testis. Among these, only eIF4E-3 has

been characterized genetically. Here, using CRISPR/Cas9 mutagenesis, we determined that eIF4E-5 is essential for male fertility. eIF4E-5 protein localizes to the distal ends of elongated spermatid cysts, and *eIF4E-5* mutants exhibit defects during post-meiotic stages, including a mild defect in spermatid cyst polarization. *eIF4E-5* mutants also have a fully penetrant defect in individualization, resulting in failure to produce mature sperm. Indeed, our data indicate that eIF4E-5 regulates non-apoptotic caspase activity during individualization by promoting local accumulation of the E3 ubiquitin ligase inhibitor Soti. Our results further extend the diversity of non-canonical eIF4Es that carry out distinct spatiotemporal roles during spermatogenesis.

Introduction

Translation of mRNA into protein is frequently targeted by genetic regulatory mechanisms (Kugler and Lasko, 2009; Lin and Holt, 2007; Mingle et al., 2005; Moor et al., 2017). Protein synthesis can be divided into three steps (initiation, elongation, termination), with much of the regulation occurring at the first step (Hershey et al., 2018; Pelletier and Sonenberg, 2019; Sonenberg and Hinnebusch, 2009). During initiation, the eukaryotic initiation factor 4F (eIF4F) cap-binding complex is recruited to the 7-methylguanylate cap located at the 5’ end of mRNAs. eIF4F is composed of a cap-binding protein (eIF4E) and an RNA helicase (eIF4A) held together by a scaffolding protein (eIF4G). eIF4G binds poly(A)-binding protein (PABP) and eIF3 to recruit the 40S ribosomal subunit. Translational repression can occur when eIF4E-binding proteins (4E-BPs) bind eIF4E to block its association with eIF4G or when eIF4E-homologous proteins (4E-HPs) bind the 5’ cap to block recruitment of eIF4E to the mRNA. Therefore, eIF4E plays an essential role in eukaryotic cap-mediated translation initiation.

Most eukaryotic genomes encode several paralogs of eIF4E whose roles and regulation are not fully understood. Mammals have three paralogs (eIF4E1 to eIF4E3; Joshi et al., 2004): mouse eIF4E1 and eIF4E2/4EHP mutants exhibit behavioral defects (Aguilar-Valles et al., 2018; Wiebe et al., 2020). *C. elegans* has five paralogs (IFE-1 to IFE-5): IFE-3, which is most similar to mammalian eIF4E1 (*i.e.*, canonical), is essential for viability; IFE-1 is required for spermatogenesis and oocyte maturation; IFE-2 is needed for meiotic recombination; and IFE-4 is required to translate mRNAs involved in egg laying (Amiri et al., 2001; Dinkova et al., 2005; Henderson et al., 2009; Kawasaki et al., 2011; Keiper et al., 2000; Song et al., 2010). *Drosophila* has eight paralogs (eIF4E-1 to eIF4E-8/4E-HP) that bind mRNA 5’ caps with varying affinities

in vitro (Zuberek et al., 2016). Canonical eIF4E-1 and 4E-HP are essential for viability, and eIF4E-3 is needed for meiotic chromosome segregation and cytokinesis during spermatogenesis (Brown et al., 2014; Chintapalli et al., 2007; Ghosh and Lasko, 2015; Hernández et al., 2012). However, the roles of the remaining paralogs are uncharacterized. Whereas *eIF4E-1* and *4E-HP* mRNAs are ubiquitously expressed, *eIF4E-3*, *eIF4E-4*, *eIF4E-5* and *eIF4E-7* mRNAs are highly and specifically enriched in the testis (Graveley et al., 2011). This suggests that these paralogs may have distinct cellular or developmental roles during sperm development.

The stages of *Drosophila* male germ cell development are organized in a spatiotemporal manner within the adult testis (Fig. S1). The stem cell niche is located at the apical tip, and germ cell development progresses toward the basal end, where mature sperm exit and are deposited in the seminal vesicle (reviewed in Fabian and Brill 2012; Fuller 1993; Lindsley and Tokuyasu, 1980; Renkawitz-Pohl et al., 2005). Male germline stem cells divide asymmetrically to form new stem cells and differentiating daughter cells that undergo four rounds of mitosis to generate cysts of 16 primary spermatocytes, which then undergo meiosis to form cysts of 64 interconnected haploid spermatids. A series of dramatic morphological changes converts spermatids into mature sperm through a process called spermiogenesis. These changes include polarization of spermatid cysts relative to the long axis of the testis, such that nuclei cluster at the basal end and flagellar axonemes, which make up the sperm tails, assemble towards the apical tip. This is accompanied by elongation of the spermatid cysts and is followed by individualization, which separates fully elongated, interconnected spermatids into individual sperm. During individualization, unneeded organelles and other cellular material are stripped from elongated spermatid cysts by an individualization complex consisting of 64 actin cones that assemble around the nuclei and move along the length of the spermatids, forming a cystic bulge whose contents eventually pinch off into a structure called the waste bag. After individualization and coiling, the mature sperm are then deposited in the seminal vesicle, where they are stored until mating.

Post-transcriptional regulation is a crucial aspect of *Drosophila* spermatogenesis. Many genes needed post-meiotically are transcribed in primary spermatocytes and translationally repressed until later stages (Jayaramaiah-Raja and Renkawitz-Pohl, 2005; Raz et al., 2022; Renkawitz-Pohl et al., 2005; Santel et al., 1997; Schäfer et al., 1993; White-Cooper, 2010; White-Cooper and Caporilli, 2013; Zhao et al., 2010). In addition, a group of “cup” and “comet” genes – named based on their mRNA distribution at the growing ends of elongating spermatid

cysts – is transcribed post-meiotically (Barreau et al., 2008a,b). One of the comet genes, *soti*, encodes a protein that controls non-apoptotic caspase activity during individualization and is needed for male fertility (Kaplan et al., 2010). By binding the testis-specific Cullin-3 ring E3 ubiquitin ligase, Soti inhibits ubiquitination and degradation of the inhibitor of apoptosis-like protein dBruce, thus preventing ectopic caspase activation (Kaplan et al., 2010). Soti is concentrated at the distal ends of elongated spermatid cysts and forms a gradient that decreases towards the spermatid heads, leading to accumulation of activated caspase near spermatid nuclei and in the cystic bulges that accompany movement of the individualization complex. Although little is known about translational control of cup and comet mRNAs, the cytoplasmic polyadenylation element binding protein (CPEB) Orb2 binds the 3' UTRs of *soti*, suggesting it might regulate *soti* translation (Xu et al., 2012). Orb2 is required for localization of *atypical protein kinase C* (*aPKC*) mRNA and protein in elongating spermatid cysts and acts with aPKC to ensure proper polarization of spermatid cysts relative to the long axis of the testis (Xu et al., 2014).

Here, we show that the testis-enriched translation initiation factor eIF4E-5 is essential for male fertility, localizes to the distal ends of elongated spermatid cysts, interacts genetically with *orb2* and *aPKC* during spermatid cyst polarization and is required for normal accumulation of Soti at the distal ends of elongated spermatids prior to individualization. Thus, eIF4E-5 is a novel player in post-transcriptional regulation during spermiogenesis.

Results

eIF4E-5 interacts with known translation regulators

To determine if eIF4E-5 can interact with known translational regulators, we used yeast two-hybrid (Y2H) assays to examine the ability of eIF4E-5 ("bait") to bind potential interactors ("prey"): the ubiquitous translation initiation factor eIF4G and testis-specific eIF4G-2, which have roles in sperm development and male fertility (Hernández et al., 1998; Baker and Fuller, 2007; Franklin-Dumont et al., 2007; Ghosh and Lasko, 2015); and the 4E-BPs Thor (also known as 4E-BP; Miron et al., 2001), 4E transporter (4E-T) (Kamenska et al., 2014), Cup (Nelson et al., 2004; Zappavigna et al., 2004), and GRB10-interacting GYF (GIGYF) (Russica et al., 2019) (Fig. 1A). Positive interactions were detected between eIF4E-5 and Thor, eIF4G-2, 4E-T, and Cup, but not eIF4G or GIGYF. The lack of interaction between eIF4E-5 and eIF4G was

unexpected, as we previously detected a weak interaction of these proteins in a more sensitive yeast two-hybrid assay (Hernández et al., 2005) and in fluorescent binding assays with a short eIF4G peptide containing the eIF4E-binding motif (Zuberek et al., 2016). Unlike binding of eIF4E-5 to Thor, 4E-T and Cup, binding to eIF4G-2 was sensitive to more stringent selection conditions, indicating that eIF4E-5 might preferentially bind inhibitors of translation rather than translational activators. These results suggest eIF4E-5 may form various complexes to regulate translation initiation during sperm development, consistent with the expected role of eIF4Es.

eIF4E-5 is required for male fertility

eIF4E-5 encodes a single predicted polypeptide of 232 amino acids that contains conserved residues needed to bind the mRNA cap (Hernández et al., 2005). To examine the role of eIF4E-5 in *Drosophila* spermatogenesis, CRISPR/Cas9-mediated mutagenesis was used to produce *eIF4E-5* alleles with deletions in the coding sequence of the gene (Fig. 1B). The deletions in *eIF4E-5*^{B8a} (12 bp), *eIF4E-5*^{B8b} (3 bp) and *eIF4E-5*^{D19a} (1 bp) are predicted to produce a 4-amino acid in-frame deletion, a 1-amino acid in-frame deletion, and a frameshift resulting in a 77-amino acid truncated protein lacking the eIF4E domain, which contains the cap-binding site (Fig. 1C). All three mutations affect the His-Pro-Leu motif that is required for binding to eIF4G and other 4E-BPs (His55, Pro56, Leu57; Grüner et al., 2016; Kinkelin et al., 2012; Peter et al., 2015): *eIF4E-5*^{B8a} removes Pro56, Leu57, Glu58, His59; *eIF4E-5*^{B8b} removes His55; and *eIF4E-5*^{D19a} has a frameshift after His55 that removes all subsequent amino acids, replacing them with 22 amino acids from an alternate reading frame. Thus, all three *eIF4E-5* mutations are predicted to interfere with eIF4G/4E-BP binding and eIF4F complex formation.

To investigate whether eIF4E-5 protein levels were reduced in these mutants, polyclonal antibodies were raised against the full-length sequence of eIF4E-5. The antibodies strongly recognized a protein at the predicted molecular weight of approximately 26.9 kDa on immunoblots of testis extracts from controls. eIF4E-5 was substantially reduced in testis extracts from *eIF4E-5*^{B8a} or *eIF4E-5*^{B8b} and undetectable in *eIF4E-5*^{D19a} homozygous mutants (Figs 1D and S2A-B). A truncated peptide of eIF4E-5, with a predicted molecular weight of approximately 8.4 kDa, was also not detectable in *eIF4E-5*^{D19a} (Fig. S2A-B). The reduced levels of eIF4E-5, potentially caused by perturbation of protein folding or eIF4F complex formation, suggest all three mutations severely reduce or abrogate eIF4E-5 function.

Males homozygous mutant for *eIF4E-5* were viable (Fig. S2C) but sterile (Fig. 1E), as were male *eIF4E-5*^{B8a}, *eIF4E-5*^{B8b} and *eIF4E-5*^{D19a} mutants *in trans* with two different deficiencies, *Df(3L)BSC631* and *Df(3L)Exel6279*, that remove the *eIF4E-5* locus. A 1610 bp genomic rescue construct containing an N-terminal 3xFLAG in frame with the eIF4E-5 coding region restored male fertility in *eIF4E-5*^{B8a}, *eIF4E-5*^{B8b} and *eIF4E-5*^{D19a} homozygous mutants. These results confirm that the male sterility of *eIF4E-5* mutants is due to loss of eIF4E-5 function rather than a second-site mutation generated by CRISPR/Cas9 mutagenesis. Closer inspection of fixed (Fig. 1F-I) and live (Figs 1J-L and S2D-F) seminal vesicles revealed that mature sperm failed to accumulate in seminal vesicles of *eIF4E-5* mutants (Fig. 1F-I) and that expression of the transgene resulted in the presence of mature, motile sperm (Figs 1J-L and S2D-F, yellow arrowheads). Hence, eIF4E-5 is required for male fertility.

eIF4E-5 localizes to the distal ends of elongated spermatid cysts

To begin to decipher the requirement for *eIF4E-5* in male fertility, we examined eIF4E-5 protein distribution during sperm development. Immunostaining revealed that eIF4E-5 (Fig. 2A-A'', yellow arrowheads) localized near the membrane skeletal protein Adducin (also called Hts; Fig. 2A-A'', insets, cyan arrowheads) at the distal ends of elongated spermatid cysts (Hime et al., 1996). Elongated spermatid cysts from *eIF4E-5*^{B8a}, *eIF4E-5*^{B8b} and *eIF4E-5*^{D19a} homozygotes retained Adducin localization (cyan arrowheads) but lacked detectible eIF4E-5 at the distal ends (Fig. 2B-D'', insets). To confirm the localization of eIF4E-5, we examined the distribution of 3xFLAG-eIF4E-5 expressed from the rescuing transgene. Immunostaining of testes from *3xFLAG-eIF4E-5;eIF4E-5*^{D19a} males with anti-FLAG and anti-eIF4E-5 antibodies revealed that tagged and endogenous eIF4E-5 were both present in the same region at the distal ends of elongated spermatid cysts (Fig. S3A-A'', insets). Testes from *eIF4E-5*^{D19a} homozygotes did not produce this pattern (Fig. S3B-B''), confirming that the signals were specific to eIF4E-5. In addition, immunostaining of testes from *3xFLAG-eIF4E-5;eIF4E-5*^{D19a} males revealed that 3xFLAG-eIF4E-5 was present in the cytoplasm of spermatocytes and elongating spermatids (Fig. S3C-C''). Testes from *eIF4E-5*^{D19a} mutants revealed non-specific staining with anti-FLAG antibodies at the tip of the testis and along a subset of elongated spermatid cysts, as well as non-specific staining with anti-eIF4E-5 antibodies in the nuclei of spermatogonia, spermatocytes and spermatids (Fig. S3B-B'',D-D''). Further supporting the antibody results, single molecule RNA

fluorescent *in situ* hybridization (smFISH) of *eIF4E-5* mRNA revealed diffuse distribution in male germ cells throughout spermatogenesis starting in spermatocytes and persisting into spermiogenesis (Fig. S3E-G), stages where we also detect specific antibody signal. Together, these results show that eIF4E-5 is expressed in early spermatocytes and persists through spermiogenesis, with eIF4E-5 protein becoming enriched at the distal ends of elongated spermatid cysts.

eIF4E-5 affects polarization of spermatid cysts

To understand how eIF4E-5 acts during spermatogenesis to ensure male fertility, we examined *eIF4E-5* mutant testes by fluorescence microscopy. At low magnification, testes from *eIF4E-5* mutants resembled wild-type testes (Fig. 3A-B). However, they exhibited spermatid cysts that were mispolarized relative to the long axis of the testis (Fig. 3A-D). In control testes, spermatid cysts with elongated nuclei (~50 cysts/testis; Zhou et al., 2011) were oriented such that all 64 nuclei within a cyst point towards the basal end of the testis and the tails point towards the apical tip (Fig. 3A,C). In contrast, in *eIF4E-5* mutants, a small subset of cysts was mispolarized relative to the long axis of the testis, such that clusters of elongated nuclei faced the apical tip (Fig. 3B, inset, yellow arrowheads, and Fig. 3D, insets; see also Fig. 2C,C'', red arrowheads). Whereas mispolarized cysts were seen in only 5% of control testes, 30-50% of *eIF4E-5* mutant testes exhibited this phenotype ($P<0.05$), which appeared to be more common in $eIF4E\text{-}5^{B8b}$ mutants than $eIF4E\text{-}5^{B8a}$ mutants (Fig. 3E). The cyst mispolarization phenotype was also observed but not quantified in $eIF4E\text{-}5^{D19a}$ mutants (L. Shao and B. Falk, unpublished observations).

The cyst polarization defect in *eIF4E-5* mutants was reminiscent of phenotypes observed in mutants for aPKC and Orb2 (Xu et al., 2014). Heterozygosity for a null allele of either *aPKC* ($aPKC^{k06403}$) or *orb2* ($orb2^{36}$) leads to mispolarized spermatid cysts, as does homozygosity for the hypomorphic $orb2^{\Delta Q}$ allele. To determine whether eIF4E-5 acts in the same manner as aPKC and Orb2, we examined testes from males transheterozygous for $eIF4E\text{-}5^{B8a}$ or $eIF4E\text{-}5^{B8b}$ and $aPKC^{k06403}$ or $orb2^{36}$ (Fig. 3F). In comparison to the single heterozygous mutants, which exhibited low levels of cyst mispolarization (7-17% of testes), this phenotype was enhanced in the transheterozygotes (29-37% testes) ($P<0.05$). These genetic results suggest eIF4E-5 acts with Orb2 and aPKC to control spermatid cyst polarization. However, because the effects of *eIF4E-5*

mutations on cyst polarity are not fully penetrant, this defect is unlikely to be the primary cause of the observed fertility defects.

eIF4E-5 is dispensable for translation of axonemal dynein

mRNA regulatory mechanisms at the distal ends of elongating spermatids are required to ensure proper flagellar axoneme assembly (Fingerhut and Yamashita, 2020). Hence, we examined whether eIF4E-5 is needed for translation of testis-specific axonemal dynein heavy chain *kl-3* mRNA, which localizes at the distal ends (Fingerhut and Yamashita, 2020). Using smFISH coupled with immunofluorescence, we found that *kl-3* mRNA (cysts with dashed outlines) did not colocalize with eIF4E-5 protein (cyan arrowheads) at the distal ends of elongating cysts (Fig. 4A-C). Immunoblotting of endogenously tagged Kl-3-3xFLAG revealed that Kl-3 protein levels were unaffected in *eIF4E-5* mutants (Fig. 4D). These results suggest translational regulation involved in axoneme assembly is likely independent of eIF4E-5.

eIF4E-5 is required for spermatid individualization

To further explore the cause of male sterility in *eIF4E-5* mutants, we examined testes by phase-contrast microscopy. Although overall testis morphology appeared normal, including the presence of elongated spermatid cysts, waste bags containing cellular material removed during individualization (Fig. 5A', cyan arrowheads) were absent, suggesting loss of eIF4E-5 caused defects in spermatid individualization (Fig. 5A-D'). Whole testes stained for activated (cleaved) caspase-3 revealed normal cystic bulges in control testes (Fig. 5E,E', yellow arrowheads), whereas these appeared flattened in *eIF4E-5* mutants (Fig. 5F-H', yellow arrowheads). The mutants also displayed an elevated level of active effector caspases throughout the lengths of the spermatid tails (Fig. 5F'-H'), as compared to control (Fig. 5E,E'). Morphology of nascent actin cones at the basal end of the testis appeared unaffected by loss of eIF4E-5, forming organized individualization complexes similar to the control (Fig. 5Ii-Li). However, in contrast to the synchronous movement of groups of 64 actin cones towards the testis tip in the control (Fig. 5I-Iiii), actin cones in *eIF4E-5* mutants appeared to scatter and become disorganized as they progressed (Fig. 5J-Liii). Waste bag formation, caspase distribution and actin cone movement were rescued by the 3xFLAG-eIF4E-5 transgene (Fig. S4A-C). Therefore, individualization initiates but ultimately fails when eIF4E-5 is absent. As individualization is an essential step in

the formation of mature sperm, this fully penetrant phenotype is likely the cause of male infertility in *eIF4E-5* mutants.

eIF4E-5 is required for localized accumulation of Soti protein

Because *eIF4E-5* and *soti* mutants show similar defects in individualization, we investigated whether Soti mRNA or protein was affected in *eIF4E-5* mutants. Although both *soti* and *kl-3* mRNAs are localized at the distal ends of early elongating spermatid cysts (Barreau et al., 2008b; Fingerhut and Yamashita, 2020), *soti* mRNA localized more distally than *kl-3* mRNA and, unlike *kl-3*, accumulated at the distal ends (Fig. S5A-C), in a manner reminiscent of eIF4E-5 protein. As loss of eIF4E-5 did not alter *soti* mRNA expression or localization (Fig. S5D-I), we further investigated whether eIF4E-5 was important for Soti protein accumulation.

In control testes, Soti was present in a gradient that was highest at the distal ends of elongated spermatid cysts (Fig. 6A, yellow arrowheads), marked by Adducin (Fig. 6A, cyan arrowheads). Soti protein appeared reduced in *eIF4E-5*^{D19a} mutants (Fig. 6B) but not absent (compare to *soti*^{sik} null mutants; Fig. 6D). Soti concentration at the distal end was rescued by expression of the 3xFLAG-eIF4E-5 genomic transgene, although not to the same level as controls (Fig. 6C, yellow arrowheads). Immunoblotting revealed that Soti protein levels were reduced in testis extracts from all three *eIF4E-5* mutants (Fig. S6). These results demonstrate that eIF4E-5 is dispensable for *soti* mRNA distribution but is nevertheless required for normal levels and accumulation of Soti protein at the distal ends of elongated spermatid cysts.

To determine the relative timing of Soti and eIF4E-5 accumulation at the distal ends of elongated cysts, we examined colocalization of Soti, eIF4E-5, and polyglycylated tubulin, a posttranslational modification of flagellar axonemes that occurs at the onset of individualization. Immunostaining revealed partial colocalization of Soti and eIF4E-5 and showed that Soti largely disappeared before individualization, whereas eIF4E-5 persisted into later stages (Fig. 7A,D). smFISH of *soti* mRNA combined with immunofluorescence of Soti and 3xFLAG-eIF4E-5 (Fig. 7B-C) confirmed that they accumulate in a sequential manner during spermiogenesis (Fig. 7D). *soti* mRNA was found at the distal ends of early elongating cysts and persisted throughout elongation (Figs 7B,Ci-Ciii, S3F,G and S5D-F). Soti protein colocalized with *soti* mRNA at the distal ends of elongated cysts and accumulated as *soti* mRNA levels declined (Fig. 7Ciii-Cv). 3xFLAG-eIF4E-5 colocalized with Soti protein and accumulated as Soti protein levels declined

(Fig. 7Cv-Cviii). Together, these results show eIF4E-5 is important for localized distribution and abundance of Soti, which is needed for caspase regulation during individualization and therefore male fertility.

Discussion

eIF4E-5 is required for spermiogenesis and male fertility

Our data indicate that eIF4E-5 is essential for *Drosophila* male fertility and is needed during at least two different stages of spermatogenesis for faithful polarization of spermatid cysts and individualization of spermatids to form mature sperm. These post-meiotic defects in *eIF4E-5* mutants are distinct from the earlier defects observed in *eIF4E-3* mutants (Hernández et al., 2012), demonstrating that two of the four testis-enriched eIF4Es have distinct spatiotemporal roles during *Drosophila* spermatogenesis. eIF4E-3 is enriched in primary spermatocytes, where it is needed for meiotic chromosome segregation and cytokinesis (Hernández et al., 2012). In contrast, eIF4E-5 concentrates at the distal end of elongated spermatid cysts, a site important for regulating individualization. Although both *eIF4E-3* and *eIF4E-5* are transcribed in primary spermatocytes, enrichment of these two eIF4E paralogs coincides with the stages they regulate, supporting the idea that evolutionary expansion of these non-canonical testis-enriched eIF4Es enabled their distinct roles and regulation during spermatogenesis. Supporting this, complementation experiments revealed that eIF4E-1 and eIF4E-3, but not eIF4E-5, are able to rescue growth of *Saccharomyces cerevisiae* lacking its only eIF4E paralog, Cdc33 (Hernández et al., 2005). These results suggest that eIF4E-1/-3 and eIF4E-5 likely have different activities or require distinct binding partners *in vivo*. Identifying paralog-specific interactors and unravelling the corresponding mechanisms will provide a better understanding of post-transcriptional regulation in *Drosophila* sperm development.

eIF4E-5 acts with aPKC and Orb2 to regulate spermatid cyst polarization

For successful transfer of mature sperm to the seminal vesicle, spermatid cysts must polarize such that nuclei face the basal end of the testis, and the tails point towards the tip. aPKC and Orb2 are involved in polarization of the cysts; heterozygous *aPKC* or *orb2* mutants exhibit bundles of 64 spermatids whose polarity is reversed relative to the long axis of the tissue (Xu et al., 2014). Orb2 ensures localization and localized translation of *aPKC* mRNA to establish

spermatid cyst polarity, and transheterozygotes of *aPKC* and *orb2* have a more severe defect than heterozygotes alone (Xu et al., 2014). Here, we show that *eIF4E-5* mutants exhibit the same polarization defect as *aPKC* and *orb2* mutants, with a subset of spermatid cysts pointing towards the wrong end of the testis. Transheterozygous mutants of *eIF4E-5* and *aPKC* or *orb2* have a more severe polarity defect than the heterozygous mutants alone, suggesting that eIF4E-5, aPKC and Orb2 might act in the same pathway to establish spermatid cyst orientation. aPKC protein localizes at the growing ends of elongating spermatids where its mRNA is also found (Xu et al., 2014), raising the possibility that *aPKC* mRNA or protein accumulation might be regulated by eIF4E-5.

In addition to localized translation of *aPKC* in spermatids, there is evidence that polarity proteins are post-transcriptionally regulated in different cellular contexts (Barr et al., 2016). For example, mammalian *Par-3* mRNA is locally translated for axonal outgrowth in embryonic rat neurons (Hengst et al., 2009; Macara et al., 2009). This raises the possibility that polarity proteins other than aPKC are similarly regulated in spermatids. Furthermore, Xu et al. (2014) described a subset of cysts as mispolarized in *par-6* heterozygotes. This suggests Par-6 might also act with eIF4E-5, aPKC and Orb2 to control spermatid cyst polarization, and its transcript could be a potential target of eIF4E-5 regulation. Our results add to the existing literature that post-transcriptional regulation plays an important role in cyst polarization during *Drosophila* spermatogenesis and indicate that eIF4E-5 participates in this process.

eIF4E-5 is needed for spermatid individualization and Soti protein accumulation

Non-apoptotic caspase activity is needed for progression of actin cones and degradation of unneeded organelles during individualization (Arama et al., 2003, 2007; Huh et al., 2004; Muro et al., 2006). In elongated spermatid cysts, caspases are initially activated at the nuclear end, where actin cones form, and repressed along the spermatid tails. As the actin cones move away from the nuclei, the peak of caspase activity remains associated with the cystic bulge. This localized caspase activity allows for controlled degradation of organelles, and disruption of this activity leads to failure of individualization, characterized by scattered actin cones. Graded distribution of Soti and dBruce along the length of elongated spermatid cysts, highest at the distal end and lowest at the nuclear end, is required for this localized caspase activation (Arama et al., 2007; Kaplan et al., 2020). In this study, we show that localized caspase activation is disrupted

and actin cones are scattered in individualizing spermatids of *eIF4E-5* mutants, resembling *soti* mutants (Kaplan et al., 2020). We also show that localized accumulation of Soti protein is reduced at the distal end of elongated spermatids in *eIF4E-5* mutants, whereas *soti* mRNA is unaffected. Collectively, these results suggest that eIF4E-5 post-transcriptionally regulates non-apoptotic caspase activity during spermiogenesis.

Although Soti protein and eIF4E-5 colocalize at the distal ends of elongated spermatid cysts, *soti* mRNA and eIF4E-5 do not. Because eIF4E-5 accumulates at the distal ends as Soti protein is reduced, eIF4E-5 likely regulates Soti levels indirectly and may directly regulate other mRNA targets that are needed for individualization. In addition to *soti*, many transcripts have been identified that are post-meiotically transcribed and accumulate at the distal ends of elongating spermatid cysts in cup or comet patterns (Barreau et al., 2008a,b; Rathke et al., 2007; Raz et al., 2022; Vibranovski et al., 2009, 2010). It is possible that one or more of these transcripts is needed for individualization and requires eIF4E-5 for its localization or localized translation. Alternatively, eIF4E-5 might promote Soti accumulation or stability independent of any role it may have in mRNA regulation. Thus, although our results reveal a novel requirement for eIF4E-5 in promoting regulation of non-apoptotic caspase activity during *Drosophila* spermatogenesis, its mechanism of action remains obscure. Distinguishing among these possibilities will be the subject of future studies.

Regulation of eIF4E-5 during spermiogenesis

Although the relationship of eIF4E-5 to aPKC translation is unclear, our data show that Soti translation does not rely solely on eIF4E-5. In addition, eIF4E-5 is dispensable for translation of at least one other transcript found at the distal ends of spermatid cysts, *kl-3*. Indeed, eIF4E-5 accumulates in elongated spermatids at a later stage than *kl-3* mRNA, at the onset of individualization when flagellar axonemes microtubules are polyglycylated. Because eIF4E-5 protein is present in the cytoplasm of male germ cells in primary spermatocytes and spermatids, and its transcript also shows a diffuse localization at these stages, it appears that localized accumulation of eIF4E-5 is through a separate mechanism from Soti localization. Thus, it remains unclear how eIF4E-5 protein becomes concentrated at the distal end. It will be of interest to identify the regulatory mechanisms involved in eIF4E-5 localization and, more broadly, mRNA translation at the distal ends of elongated spermatid cysts.

Our results indicate that eIF4E-5 directly binds several known eIF4E binding partners (Thor, eIF4G-2, 4E-T, Cup) and might act in the same pathway as Orb2. Interactions with these proteins may facilitate or repress translational activity of eIF4E-5 on its target mRNAs at different stages of spermiogenesis. Although canonical eIF4E-1 and testis-specific eIF4E-3 associate with canonical eIF4G and testis-specific eIF4G-2 (Hernández et al., 2012), eIF4E-5 shows a stronger interaction with eIF4G-2 than eIF4G. Thus, an eIF4F complex formed by eIF4E-5 and eIF4G-2 might target transcripts for translation *in vivo*. Despite apparent differences between *Drosophila* and human spermatogenesis, activation of pro-apoptotic proteins without causing the death of the entire cell is also used to eliminate cytoplasmic components during terminal differentiation of mammalian spermatids (Shaha et al., 2010). Because one known cause of human male infertility is incomplete extrusion of sperm cytoplasm (Rengan et al., 2012), it would be of interest to know if there is a similar role for post-transcriptional regulation in this aspect of male fertility in humans.

Materials and Methods

Fly strains and husbandry

Flies were raised on standard cornmeal molasses agar at 25°C (Ashburner, 1990). w^{1118} and y^{1} w^{1} were used as experimental controls. w^{1118}; *PBac{vas-Cas9}* (Bloomington Drosophila Stock Center (BDSC) #56552, Bloomington, USA) was used to generate *eIF4E-5* CRISPR/Cas9 mutants. y^{1} *M{3xP3-RFP-3xP3-GFP-vas-int.DM}ZH-2A* w^{*}*; P{CaryP}attP40* (BestGene Inc.) contains a second chromosome attP site (25C6) and was used to generate 3xFLAG-eIF4E-5 transgenic lines. Double-balancer stock w^{1118}; *Sco/CyO*; *MKRS/TM6B* was used for balancing mutants. *eIF4E-5* alleles were examined *in trans* to chromosomal deletions *Df(3L)BSC631* (BDSC #25722) and *Df(3L)Exel6279* (BDSC #7745) lacking the entire *eIF4E-5* coding region. *kl-3*^{3xFLAG} carries a 3xFLAG tag at the endogenous C-terminus of the *kl-3* coding region, generated by CRISPR/Cas9-mediated knock-in (Fingerhut et al., 2019). *UAS-kl-3*$^{TriP.HMC03546}$ (BDSC #53317) expresses dsRNA for RNAi directed against *kl-3* under UAS control (Perkins et al., 2015). *bam-GAL4:VP16* expresses the GAL:VP16 driver under control of the *bam* promoter (BDSC #80579; Chen and McKearin, 2003). *aPKC*^{k06403} (BDSC #10622) carries a *P{lacW}* insertion between two promoters in the third intron, resulting in a loss of function allele (Xu et al., 2014). *orb2*^{36} (BDSC #58479) carries a deletion of the Orb2 coding region generated through

FRT-mediated recombination between two flanking progenitor insertions of *PBac{WH}CG43783*^{f04965} and *PBac{WH}orb2*^{f01556} (Xu et al., 2012). *Soti*^{sik} (BDSC #32124) contains an imprecise excision of *P{XP}d01837* that compromises the promoter and coding regions of *soti* (Kaplan et al., 2010).

Fertility tests were performed by mating individual males of each genotype with five virgin w^{1118} females at 25°C. After 5 days, crosses were observed for the presence of progeny. For the rescue experiments, fertility tests were performed by mating individual males of each *eIF4E-5* mutant expressing *3x-FLAG-eIF4E-5* transgene with three virgin w^{1118} females at 25°C. After 14 days, crosses were observed for presence of progeny.

Viability tests were performed by mating three males and three females heterozygous for each mutant allele over the *TM6B* balancer chromosome at 25°C. After 10 days, progeny were scored for absence or presence of the balancer and compared with the expected Mendelian ratio to determine eclosion rates. Differences observed between mutant allele ratios and the expected ratio were analyzed with one way ANOVA with Dunnett's multiple comparison test. Results were considered statistically significant at $P<0.05$. Two replicates were performed for *eIF4E-5*^{B8a} and *eIF4E-5*^{D19a}, and four replicates were performed for *eIF4E-5*^{B8b}.

Generation of *eIF4E-5* mutant strains

Guide (gRNAs) targeting two different regions in *eIF4E-5* with no predicted off-targets were selected using the CRISPR Optimal Target Finder (http://targetfinder.flycrispr.neuro.brown.edu; Gratz et al., 2014): 5'-GAATTTTGTCGCGATTCGAG-3' (gRNA1) and 5'-GAGTCGAGTACAAGCATCCTT-3' (gRNA2). The two selected gRNAs were cloned into pCFD4d under two promoters, U6-1 and U6-3 (Addgene plasmid #83954, Watertown, USA; Ge et al., 2016). pCFD4d was digested with *Bbs*I (New England Biolabs, R3539L, Waltham, USA) and gel purified. Inserts were generated by PCR using the following primers and pCFD4d as a template: 5'-TATATAGGAAAGATATCCGGGTGAACTTCGGAATTTTGTCGCGATTCGAGGTTTTAGAGCTAGAAATAGCAAG-3' and 5'-ATTTTAACTTGCTATTTCTAGCTCTAAAACAAGGATGCTTGTACTCGACTCGACGTTAAATTGAAAATAGGTC-3'. The backbone and insert were combined by Gibson Assembly Master Mix (New England Biolabs, E2611L). The gRNA plasmid was confirmed by sequencing,

injected into transgenic embryos expressing Vasa-Cas9 and allowed to develop to adulthood (BestGene Inc., Chino Hills, USA). Each adult fly was individually crossed with a balancer stock to generate stocks of putative mutants. Genomic DNA was extracted from homozygous putative mutants of each stock for PCR amplification of *eIF4E-5* and sequenced using primers: 5'-GGTGATGACACTACTGACGC-3' and 5'-AACGCCCAACAAACTGAAAC-3' (The Centre for Applied Genomics, The Hospital for Sick Children, Toronto, Canada). This experiment was repeated twice; the initial round identified two different mutant alleles from the same founder parent (*eIF4E-5*^{B8a} and *eIF4E-5*^{B8b}) and the second round identified a frameshift allele (*eIF4E-5*^{D19a}). Fly stocks and plasmids described here are available upon request.

Generation of genomic 3xFLAG-eIF4E-5 rescue construct and transgenic flies

The rescue construct consisted of genomic DNA corresponding to the *eIF4E-5* locus, starting 359 bp upstream of the ATG, 69 bp 3xFLAG tag (5'-GACTACAAAGACCATGACGGTGATTATAAAGATCATGACATCGATTACAAGGATGACGATGACAAG-3'), 12 bp linker (5'- GGCAGCGAATTC-3'), all 791 bp of eIF4E-5 protein coding sequence including introns, and 362 bp downstream of the stop codon including the putative poly(A) site. The first three regions (5' region, 3xFLAG, linker) were synthesized (BioBasic Inc., Markham, Canada) and subcloned into the pattB plasmid (Drosophila Genomics Research Center (DGRC), 1420, Bloomington, USA) using *Bam*HI (New England Biolabs, R3136S) and *Eco*RI (New England Biolabs, R3101S). The last two regions were PCR-amplified from genomic DNA with *Eco*RI and *Not*I sites (New England Biolabs, R3189S) added to the primers (5'-ATGACAAGGGCAGCGAATTCATGGCCAGTGCACAAGTG -3'and 5'-GTACCCTCGAGCCGCGGCCGCGCTTGAGTAGGCAATTACGAC-3'), cut with *Eco*RI and *Not*I (New England Biolabs, R3189S), and subcloned into pattB downstream and in-frame with the 5' genomic region, 3xFLAG and linker. The pattB-3xFLAG-eIF4E-5 plasmid was confirmed by sequencing and integrated into the attP40 site on the second chromosome via PhiC31 integrase-mediated transgenesis by injection into *y*^{1} *M{3xP3-RFP-3xP3-GFP-vas-int.DM}ZH-2A w***; P{CaryP}attP40* embryos (BestGene Inc.). Fly stocks and plasmids described here are available upon request.

Generation of anti-eIF4E-5 antibodies

The full-length coding region of *eIF4E-5* was PCR-amplified using the plasmid 4E5-pCR2.1 as a template (Hernández et al., 2005) and subcloned into pRSET (Invitrogen, V35120) to create an expression construct. The plasmid was transformed into *E. coli* BL21 (DE3) (Novagen, 71012) to produce a 6XHis fusion recombinant protein according to the manufacturer's instructions. The fusion protein was purified using Ni-NTA beads under denaturing conditions (Thermo Fisher Scientific, R90101, Waltham, USA). Polyclonal anti-eIF4E-5 antibodies were raised in rabbit against this recombinant protein (Comparative Medicine and Animal Resources Centre, McGill University, Montreal, Canada). The sera were separated and NaN_3 was added at a concentration of 0.02%. Antibodies described here are available upon request.

Squashed preparations of *Drosophila* testes

Testes were dissected from 0 to 2-day old males (unless otherwise stated) in cold testis isolation buffer (TIB) (Casal et al., 1990). Whole testes were mounted on polylysine-coated slides in TIB and squashed with a coverslip (Polysine, P4681-001, Thermo Fisher Scientific). Live images of waste bags for Fig. 5 were acquired on an upright Zeiss Axioplan 2E epifluorescence microscope equipped with a 20x phase-contrast objective and an Axiocam black and white CCD camera using Axiovision software (Carl Zeiss, Oberkochen, Germany). Live images of seminal vesicles for Fig. S2 were acquired on an inverted Leica DMi8 epifluorescence microscope equipped with a 20x phase-contrast objective and a Leica K5 camera using Thunder Imaging System. All images were uniformly processed for brightness and contrast using Adobe Photoshop (San Jose, USA).

Immunohistochemistry

Two methods were used for immunohistochemistry. Except for those in Fig. 6, testes (5-10 pairs/experiment, unless otherwise specified) were prepared as for live microscopy (above) and processed for immunofluorescence as previously described (Hime et al., 1996). In brief, after mounting on polylysine-coated slides (Polysine, Thermo Fisher Scientific, P4681-001, Waltham, USA), samples were squashed with a coverslip and frozen in liquid nitrogen. Coverslips were removed with a razor blade, and samples were immediately chilled in 95% ethanol for at least 10

minutes. Samples were fixed in PBS with 4% paraformaldehyde (Electron Microscope Sciences, 15710, Hadfield, USA) for 7-10 min, permeabilized in PBS with 0.37% Triton X-100 and 0.3% sodium deoxycholate for 30 min and blocked in PBS with 0.1% Triton X-100 and 5% bovine serum albumin (PBTB; Sigma-Aldrich, A3912-100G, St. Louis, USA). Samples were incubated at 4°C overnight with primary antibodies, washed with PBTB three times for 5 min and once for 15 min, and incubated for 1 h at room temperature with secondary antibodies diluted in PBTB. Samples were then washed with PBTB once for 15 min, stained (when applicable) with rhodamine-phalloidin in PBTB (1:200; Invitrogen, R415) for 30 min, washed with PBS with 0.1% Triton X-100 (PBT) for 15 min stained with 4',6-diamidino-2-phenylindole (DAPI) in PBT (1:1000; VWR, 89139-054, Radnor, USA) for 10 min and washed with PBT twice for 15 min. Samples were mounted in ProLong Diamond Antifade Mountant (Molecular Probes, P36961, Eugene, USA), sealed with nail polish, and examined within 1-2 days. Fluorescence micrographs were acquired on a Nikon A1R inverted laser scanning confocal equipped with 10x, 20x, 40x, and 60x objectives, photomultiplier tube (PMT) detectors for DAPI channel, and gallium arsenide phosphide (GaAsP) PMT detectors for green and red channels using NIS Elements software (SickKids Imaging Facility, The Hospital for Sick Children, Toronto, Canada). All images were uniformly processed for brightness and contrast using Adobe Photoshop (San Jose, USA).

For Fig. 6, immunohistochemistry was carried out as described above except that testes (6 pairs/experiment) were dissected in cold PBS, fixed for 30 min permeabilized, blocked, washed, and stained in membrane lined trays placed on a shaker before being mounted onto polylysine-coated slides in Vectashield Antifade Mounting Medium with DAPI (Vector Laboratories, Burlingame, USA).

Primary antibodies used for immunofluorescence were rabbit anti-eIF4E-5 (1:500; #4524, this work), rabbit anti-caspase-3 (1:400; Asp175, Cell Signaling Technology, Danvers, USA), guinea pig anti-Soti (1:100; Kaplan et al., 2010; a kind gift of Eli Arama, Weitzmann Institute, Rehovot, Israel), mouse anti-Adducin 1B1 (1:20; Zaccai and Lipshitz, 1996; a kind gift of Howard Lipshitz, University of Toronto, Toronto, Canada), mouse anti-FLAG (1:200; M2, Sigma-Aldrich, F1804) and mouse anti-polyglycylated tubulin (1:2500; clone AXO49, a gift of Marie-Hélène Bré, University of Paris-Sud, France; Bré et al., 1998). Secondary antibodies used for immunofluorescence were Alexa Fluor 488-conjugated anti-rabbit (1:1000; Invitrogen, A-

11008), Alexa Fluor 488-conjugated anti-guinea pig (1:1000; Invitrogen, A-11073), Alexa Fluor 568-conjugated anti-mouse IgG (1:1000; Invitrogen, A-31043), or Alexa Fluor 633-conjugated anti-guinea pig IgG (1:1000; Invitrogen, A-21105).

Quantifying spermatid cyst polarity defects

Testes were dissected and stained following the immunohistochemistry protocol described above. The percentage of testes with spermatid nuclei near the tip was recorded (Xu et al., 2014). For Fig. 3E-F, statistical analysis and graphing were performed using GraphPad Prism versions 8 for Macintosh, respectively (GraphPad Software). Differences observed between genotypes were analyzed with unpaired two-tailed Student *t*-test. Results were considered statistically significant at $P<0.05$. Note that *eIF4E-5*^{D19a} was isolated six months after *eIF4E-5*^{B8a} and *eIF4E-5*^{B8b} and was not included in these experiments.

Immunofluorescence with single molecule RNA FISH

All solutions used were RNase free. Testes (15-20 pairs/experiment) were dissected in 1xPBS (Invitrogen, AM9624) and fixed in 4% formaldehyde (Polysciences, Inc., 18814-10) in 1xPBS for 30 min, washed briefly in PBS, and permeabilized in 70% ethanol overnight at 4°C. Samples were then washed with 1xPBS and blocked for 30 min at 37°C in blocking buffer (1xPBS, 0.05% BSA [Invitrogen, Am2616], 50µg/mL yeast tRNA [Sigma-Aldrich, R8759], 10mM Vanadyl Ribonucleoside complex [New England Biolabs, S1402S], 0.2% Tween-20 [Sigma-Aldrich, P7949]). Samples were incubated with primary antibodies diluted in blocking buffer overnight at 4°C, washed with 1xPBS containing 0.2% Tween-20, re-blocked for 5 min at 37°C in blocking buffer, and incubated 4°C overnight in blocking buffer containing secondary antibodies. Testes were then washed with 1xPBS containing 0.2% Tween-20, and re-fixed for 10 min before being briefly rinsed with wash buffer (2x saline-sodium citrate [SSC, Invitrogen, AM9770], 10% formamide [Fisher Scientific, BP227]), and then hybridized overnight at 37°C in hybridization buffer (2xSSC, 10% dextran sulfate [Sigma-Aldrich, D8906], 1mg/mL yeast tRNA, 2mM Vanadyl Ribonucleoside complex, 0.5% BSA, 10% formamide). Following hybridization, samples were washed three times in wash buffer for 20 min each at 37°C and mounted in Vectashield with DAPI (Vector Laboratory, H-1200, Burlingame, USA). Images were acquired using an upright Leica Stellaris 8 confocal microscope with a 63X oil immersion

objective lens (NA = 1.4) and processed using ImageJ software (National Institutes of Health, Bethesda, USA).

Primary antibodies were rabbit anti-eIF4E-5 (1:500; #4524, this work) or rabbit anti-FLAG (1:500; Invitrogen, PA1-984B), and secondary antibodies were Alexa Fluor 488-conjugated anti-rabbit (1:200; Life Technologies, Carlsbad, USA). Fluorescently labeled probes were added to the hybridization buffer to a final concentration of 100nM. Probes against *kl-3*, *soti*, and *eIF4E-5* mRNA were designed using the Stellaris® RNA FISH Probe Designer (Biosearch Technologies, Inc., Novato, USA) available online at www.biosearchtech.com/stellarisdesigner. Probe sets are listed in Table S1.

For smFISH alone, hybridization immediately followed the overnight incubation in 70% ethanol and short wash with wash buffer.

Immunoblotting

Three methods were used for immunoblotting. For Figs 1 and S2, testes (20 pairs/sample) were dissected in TIB with protease inhibitor cocktail (1:100; Halt, Thermo Fisher Scientific, 87786), then lysed in radioimmunoprecipitation assay (RIPA) buffer with protease inhibitors (150 mM NaCl, 50 mM Tris-HCl pH 8.0, 1% Nonidet P-40, 0.5% sodium deoxycholate, 0.1% SDS). NuPAGE LDS Sample Buffer was added, and samples were heated for 10 min at 98°C (Invitrogen, NP0007). Proteins were run on gradient pre-cast SDS polyacrylamide gels (8-16%, ExpressPlu, GenScript, M81610, Piscataway, USA) before being transferred to nitrocellulose membranes (0.45µm, Amersham Protran, GE Healthcare Life Sciences, 10600020 Chicago, USA) with NuPAGE Transfer Buffer (Invitrogen, NP0006). Membranes were rinsed in TBST (Tris-buffered saline with 0.05% Tween-20), blocked in TBST containing 5% nonfat milk, and incubated overnight at 4°C with primary antibodies diluted in TBST containing 5% nonfat milk. Membranes were washed with TBST and incubated with secondary antibodies diluted in TBST containing 1% nonfat milk. Membranes were washed with TBST, and detection was performed using Novex ECL Chemiluminescent Substrate Reagents Kit (Invitrogen, WP20005). Primary antibodies used were rabbit anti-eIF4E-5 (1:5000; #4524, this work) and mouse anti-α-tubulin (5ug/mL; AA4.3, Developmental Studies Hybridoma Bank (DSHB), Iowa City, USA). Secondary antibodies were HRP-conjugated anti-rabbit (1:10,000; Jackson ImmunoResearch

Laboratories, 111-035-003, West Grove, USA) or anti-mouse IgG (1:10,000; Jackson ImmunoResearch Laboratories, 715-035-150).

For Fig. 4D, testes (40 pairs/sample) were dissected in Schneider's medium (Gibco, 21720-024) at room temperature within 30 minutes, the medium was removed, and samples were frozen at -80°C until use. Tissues were then lysed in equal volumes of 2xLaemmli Sample Buffer (Bio-Rad Laboratories, 1610737, Hercules, USA) + βME (Bio-Rad Laboratories, 1610710, Hercules, USA) and equal volumes were run on a NuPAGE Tris-Acetate gel (3-8%, 1.5mm, Invitrogen, EA0378BOX) with Tris-Acetate SDS Running Buffer (Invitrogen, LA0041) before being transferred onto polyvinylidene fluoride (PVDF) membrane (Bio-Rad Laboratories, 1620177, Hercules, USA) using NuPAGE transfer buffer (Invitrogen, NP0006) without added methanol. Membranes were blocked in TBST (0.1% Tween-20) containing 5% nonfat milk (Bio-Rad, 1706404, Hercules, USA), followed by incubation with primary antibodies diluted in TBST containing 5% nonfat milk. Membranes were then washed with TBST, followed by incubation with secondary antibodies diluted in TBST containing 5% nonfat milk. After washing with TBST, detection was performed using the Pierce ECL Western Blotting Substrate enhanced chemiluminescence system (Thermo Fisher Scientific, 32106). Primary antibodies used were mouse anti-α-tubulin (1:2,000; clone DM1a, Sigma-Aldrich) and mouse anti-FLAG (1:2,500; M2, Sigma-Aldrich). Secondary antibody was HRP-conjugated anti-mouse IgG (1:10,000; Abcam, ab6789, Cambridge, UK).

For Fig. S6, testes (20 pairs/sample) were dissected in PBS with protease inhibitor (Thermo Fisher Scientific, A32963). Tissues were boiled in equal volumes of PBS, protease inhibitor and 5xloading buffer (3.7mM Bromophenol Blue, 0.5M DDT, 0.3mM SDS, 0.25mM Tris pH6.8, 50% Glycerol, and 5% βME) at 98°C for 5 min and frozen overnight. Proteins were run on 10% SDS-polyacrylamide gels and transferred onto the PVDF membrane (Bio-Rad Laboratories, 162-0177) with Tris-Glycine transfer buffer (20% methanol, 25mM Tris, 0.2 M glycine). Membranes were rinsed in TBST (0.1% Triton X-100), blocked in TBST containing 5% nonfat milk, and incubated overnight at 4°C with primary antibodies diluted in blocking solution. Membranes were washed with TBST and incubated with secondary antibodies diluted in TBST containing 1% nonfat milk. Membranes were washed with TBST, and detection was performed using Novex ECL Chemiluminescent Substrate Reagents Kit (Invitrogen, WP20005). Detection was performed using SuperSignal West Femto Maximum Sensitivity Substrate Kit

(Thermo Fisher Scientific, 34095). Primary antibodies used were guinea pig anti-Soti (1:500; Kaplan et al, 2010) and mouse anti-Lamin C (DSHB, LC28.26). Secondary antibodies used were HRP-conjugated goat anti-guinea pig (1:5000; A18769, Invitrogen) or goat anti-mouse IgG (1:5000; Bio-Rad Laboratories, 170-6516).

Yeast two-hybrid assays

A cDNA encoding *Drosophila* eIF4E-5 (CG8277) was amplified by PCR using the plasmid 4E5-pCR2.1 as a template (Hernández et al., 2005) and subcloned into the vector pOAD ("prey" vector; Cagney et al., 2000) in frame with the activator domain sequence of GAL4 to generate the construct eIF4E-5-AD. *Drosophila* GIGYF (CG11148; Russica et al., 2019; a kind gift of Catia Igreja, Max Planck Institute for Developmental Biology, Tübingen, Germany), Cup (CG11181; Nelson et al., 2004; Zappavigna, et al., 2004; a kind gift of Nancy Standart, Cambridge University, Cambridge, UK), 4E-T (CG32016), eIF4G (CG10811; Hernández et al., 1998), eIF4G-2 (CG10192; Baker and Fuller 2007), and Thor (4E-BP/CG8846; Miron et al., 2001) cDNAs were subcloned into the pOBD2 vector ("bait" vector; Cagney et al., 2000) in-frame with the DNA-binding domain sequence of GAL4 to create the respective plasmids pGIGYF-BD, pCUP-BD, p4E-T-BD, peIF4G-2 (313-1164)-BD, peIF4G-BD and pThor-BD. Plasmids described here are available upon request.

Interactions between proteins expressed as "prey" or "bait" fusions were detected following a yeast interaction-mating method using the strains PJ69-4a and PJ69-4α containing reporter genes *HIS3* and *ADE2* (Cagney et al., 2000). Diploid cells containing both bait and prey plasmids were grown in –Trp, –Leu selective media (Clontech, 630417, Mountain View, USA) and shown as controls for growth. Protein interactions were detected by replica-plating diploid cells onto –Trp, –Leu, –Ade (20 ug/mL L-His HCl monohydrate (A-9126, Sigma) added to –Trp, –Leu, –Ade, –His (630428, Clontech) or –Trp, –Leu, –His (630419, Clontech) selective media +3 mM, 10 mM or 30 mM 3-amino-1,2,4-triazole (3AT, Sigma-Aldrich). Growth was scored after 4 days of growth at 30°C.

Acknowledgments

The authors are grateful to Brill lab members Jonathan Ma, Nigel Giffiths, Lacramioara Fabian, Alind Gupta and Yonit Bernstein for their support and assistance with experimental methods. We

thank Eli Arama, Howard Lipshitz and Marie-Helène Bré for antibodies. We also thank Howard Lipshitz, Craig Smibert, James Ellis, Julie Forman-Kay, Robert Vernon and Josefa Steinhauer for helpful discussions, Helen White-Cooper and Andreas Jenny for insightful comments on the manuscript, Timothy Low for advice on western blotting, Paul Paroutis and Kimberly Lau of the SickKids Imaging facility for advice on imaging, and the Bloomington Drosophila Stock Center for fly stocks. Some data were previously described or presented in a published thesis (Shao, 2019): generation of *eIF4E-5* mutant alleles and anti-eIF4E-5 antibodies; localization of eIF4E-5; infertility, mispolarized cysts, failure of individualization, disrupted caspase regulation, and reduced Soti levels in *eIF4E-5* mutants. Images have been retaken or are presented differently, and text has been rewritten.

Conflict of interest

The authors declare no competing interests.

Author contributions

Conceptualization, L.S., J.A.B.; Methodology, L.S., J.M.F., B.L.F., H.H., G.M., Y.Q., V.L., E.H., L.C., G.P., G.H., P.L., J.A.B.; Validation, L.S., J.M.F., B.L.F., G.M., G.H., J.A.B.; Formal analysis, L.S., J.M.F., B.L.F., J.A.B.; Investigation, L.S., J.M.F., B.L.F., G.M., V.L., E.H., L.C., J.A.B.; Resources, H.H., P.L.; Writing – original draft, L.S., J.A.B.; Writing – review and editing, all authors; Visualization, L.S., J.M.F., B.L.F., G.M., G.H., J.A.B.; Supervision, L.S., G.P., G.H., P.L., J.A.B; Project administration, L.S., J.A.B.; Funding acquisition, G.H., P.L., J.A.B.

Funding

This research was supported by SickKids Restracomp and Ontario Graduate Scholarships (to L.S.); National Council of Science and Technology (CONACyT) Ph.D. fellowship #749487 (to G.M.); intramural funding program of the Instituto Nacional de Cancerología, Mexico (to G.H.); CIHR Research Grant #IOP-107945 (to P.L.); and NSERC Discovery (#RGPIN-2016-06775 and #RGPIN-2022-05163) and Research Tools and Instruments (#RTI-2019-00361) grants (to J.A.B.).

References

Amiri, A., Keiper, B.D., Kawasaki, I., Fan, Y., Kohara, Y., Rhoads, R.E. and Strome, S. (2001). An isoform of eIF4E is a component of germ granules and is required for spermatogenesis in *C. elegans*. *Development* **128**, 3899-3912.

Aguilar-Valles, A., Haji, N., De Gregorio, D., Matta-Camacho, E., Eslamizade, M.J., Popic, J., Sharma, V., Cao, R., Rummel, C., Tanti, A., et al. (2018). Translational control of depression-like behavior via phosphorylation of eukaryotic translation initiation factor 4E. *Nat Commun*, **25**, 2459.

Arama, E., Agapite, J. and Steller, H. (2003). Caspase activity and a specific cytochrome C are required for sperm differentiation in *Drosophila*. *Dev. Cell* **4**, 687-697.

Arama, E., Bader, M., Rieckhof, G.E. and Steller, H. (2007). A ubiquitin ligase complex regulates caspase activation during sperm differentiation in *Drosophila*. *PLoS Biol.* **5**, e251.

Ashburner, M. (1990). *Drosophila*: A laboratory handbook (Cold Spring Harbor, NY: Cold Spring Harbor Press).

Baker, C.C. and Fuller, M.T. (2007). Translational control of meiotic cell cycle progression and spermatid differentiation in male germ cells by a novel eIF4G homolog. *Development* **134**, 2863-2869.

Barr, J., Yakovlev, K.V., Shidlovskii, Y. and Schedl, P. (2016). Establishing and maintaining cell polarity with mRNA localization in *Drosophila*. *BioEssays* **38**, 244-253.

Barreau, C., Benson, E., Gudmannsdottir, E., Newton, F. and White-Cooper, H. (2008a). Post-meiotic transcription in *Drosophila* testes. *Development* **135**, 1897-1902.

Barreau, C., Benson, E. and White-Cooper, H. (2008b). Comet and cup genes in *Drosophila* spermatogenesis: the first demonstration of post-meiotic transcription. *Biochem. Soc. Trans.* **36**, 540-542.

Bré, M.H., Redeker V., Vinh J., Rossier J. and Levilliers, N. (1998). Tubulin polyglycylation: differential posttranslational modification of dynamic cytoplasmic and stable axonemal microtubules in paramecium. *Mol. Biol. Cell* **9**, 2655–2665.

Cagney, G., Uetz, P. and Fields, S. (2000). High-throughput screening for protein-protein interactions using two-hybrid assay. *Methods Enzymol.* **328**, 3-14.

Casal, J., Gonzalez, C., Wandosell, F., Avila, J. and Ripoll, P. (1990). Abnormal meiotic spindles cause a cascade of defects during spermatogenesis in asp males of *Drosophila*. *Development* **108**, 251-260.

Chen, D. and McKearin, D.M. (2003). A discrete transcriptional silencer in the bam gene determines asymmetric division of the *Drosophila* germline stem cells. *Development* **130**, 1159-1170.

Dinkova, T.D., Keiper, B.D., Korneeva, N.L., Aamodt, E.J. and Rhoads, R.E. (2005). Translation of a small subset of *Caenorhabditis elegans* mRNAs is dependent on a specific eukaryotic translation initiation factor 4E isoform. *Mol. Cell. Biol.* **25**, 100-113.

Fabian, L. and Brill, J.A. (2012). *Drosophila* spermiogenesis: big things come from little packages. *Spermatogenesis* **2**, 197-212.

Fingerhut, J.M., Moran, J.V. and Yamashita, Y.M. (2019). Satellite DNA-containing gigantic introns in a unique gene expression program during *Drosophila* spermatogenesis. *PLoS Genet.* **15**, e1008028.

Fingerhut, J.M. and Yamashita, Y.M. (2020). mRNA localization mediates maturation of cytoplasmic cilia in *Drosophila* spermatogenesis. *J. Cell Biol.* **219**, e202003084.

Franklin-Dumont, T.M., Chatterjee, C., Wasserman, S.A. and DiNardo, S. (2007). A novel eIF4G homolog, Off-schedule, couples translational control to meiosis and differentiation in *Drosophila* spermatocytes. *Development* **134**, 2851-2861.

Fuller, M.T. (1993). Spermatogenesis (Cold Spring Harbor, NY: Cold Spring Harbor Press).

Ge, D.T., Tipping, C., Brodsky, M.H. and Zamore, P.D. (2016). Rapid screening for CRISPR-directed editing of the *Drosophila* genome using *white* co-conversion. *G3 (Bethesda)* **6**, 3197-3206.

Ghosh, S. and Lasko, P. (2015). Loss-of-function analysis reveals distinct requirements of the translation initiation factors eIF4E, eIF4E-3, eIF4G and eIF4G2 in *Drosophila* spermatogenesis. *PLoS ONE* **10**, e0122519.

Gratz, S.J., Ukken, F.P., Rubinstein, C.D., Thiede, G., Donohue, L.K., Cummings, A.M. and O'Connor-Giles, K.M. (2014). Highly specific and efficient CRISPR/Cas9-catalyzed homology-directed repair in *Drosophila*. *Genetics* **196**, 961-971.

Graveley, B.R., Brooks, A.N., Carlson, J.W., Duff, M.O., Landolin, J.M., Yang, L., Artieri, C.G., van Baren, M.J., Boley, N., Booth, B.W., et al. (2011). The developmental transcriptome of *Drosophila melanogaster*. *Nature* **471**, 473-479.

Grüner, S., Peter, D., Weber, R., Wohlbold, L., Chung, M., Weichenrieder, O., Valkov, E., Igreja, C. and Izaurralde, E. (2016). The structures of eIF4E-eIF4G complexes reveal an extended interface to regulate translation initiation. *Mol. Cell* **64**, 467-479.

Henderson, M.A., Cronland, E., Dunkelbarger, S., Contreras, V., Strome, S. and Keiper, B.D. (2009). A germline-specific isoform of eIF4E (IFE-1) is required for efficient translation of stored mRNAs and maturation of both oocytes and sperm. *J. Cell Sci.* **122**, 1529-1539.

Hengst, U., Deglincerti, A., Kim, H.J., Jeon, N.L. and Jaffrey, S.R. (2009). Axonal elongation triggered by stimulus-induced local translation of a polarity complex protein. *Nat. Cell Biol.* **11**, 1024-1030.

Hernández, G., Altmann, M., Sierra, J.M., Urlaub, H., Diez del Corral, R., Schwartz, P. and Rivera-Pomar, R. (2005). Functional analysis of seven genes encoding eight translation initiation factor 4E (eIF4E) isoforms in *Drosophila*. *Mech. Dev.* **122**, 529-543.

Hernández, G., Castellano, M.M., Agudo, M. and Sierra, J.M. (1998). Isolation and characterization of the cDNA and the gene for eukaryotic translation initiation factor 4G from *Drosophila melanogaster*. *Eur. J. Biochem.* **253**, 27-35.

Hernández, G., Han, H., Gandin, V., Fabian, L., Ferreira, T., Zuberek, J., Sonenberg, N., Brill, J.A. and Lasko, P. (2012). Eukaryotic initiation factor 4E-3 is essential for meiotic chromosome segregation, cytokinesis and male fertility in *Drosophila*. *Development* **139**, 3211-3220.

Hernández, G., Vázquez-Pianzola, P., Sierra, J.M. and Rivera-Pomar, R. (2004). Internal ribosome entry site drives cap-independent translation of *reaper* and *heat shock protein 70* mRNAs in *Drosophila* embryos. *RNA* **10**, 1783-1797.

Hershey, J.W.B., Sonenberg, N. and Mathews, M.B. (2019). Principles of translational control. *Cold Spring Harb. Perspect. Biol.* **11**, a032607.

Hime, G.R., Brill, J.A. and Fuller, M.T. (1996). Assembly of ring canals in the male germ line from structural components of the contractile ring. *J. Cell Sci.* **109**, 2779–2788.

Huh, J.R., Vernooy, S.Y., Yu, H., Yan, N., Shi, Y., Guo, M. and Hay, B.A. (2004). Multiple apoptotic caspase cascades are required in nonapoptotic roles for *Drosophila* spermatid individualization. *PLoS Biol.* **2**, E15.

Jayaramaiah-Raja, S. and Renkawitz-Pohl, R. (2005). Replacement by *Drosophila melanogaster* protamines and Mst77F of histones during chromatin condensation in late spermatids and role of sesame in the removal of these proteins from the male pronucleus. *Mol. Cell. Biol.* **25**, 6165-6177.

Joshi, B., Cameron, A. and Jagus, R. (2004). Characterization of mammalian eIF4E-family members. *Eur. J. Biochem.* **271**, 2189-2203.

Kamenska, A., Lu, W.T., Kubacka, D., Broomhead, H., Minshall, N., Bushell, M. and Standart, N. (2014). Human 4E-T represses translation of bound mRNAs and enhances microRNA-mediated silencing. *Nucleic Acids Res.* **42**, 3298-3313.

Kaplan, Y., Gibbs-Bar, L., Kalifa, Y., Feinstein-Rotkopf, Y. and Arama, E. (2010). Gradients of a ubiquitin E3 ligase inhibitor and a caspase inhibitor determine differentiation or death in spermatids. *Dev. Cell* **19**, 160-173.

Kawasaki, I., Jeong, M. and Shim, Y. (2011). Regulation of sperm-specific proteins by IFE-1, a germline-specific homolog of eIF4E, in *C. elegans*. *Mol. Cells* **31**, 191-197.

Keiper, B.D., Lamphear, B.J., Deshpande, A.M., Jankowska-Anyszka, M., Aamodt, E.J., Blumenthal, T. and Rhoads, R.E. (2000). Functional characterization of five eIF4E isoforms in *Caenorhabditis elegans*. *J. Biol. Chem.* **275**, 10590-10596.

Kinkelin, K., Veith, K., Grünwald, M. and Bono, F. (2012) Crystal structure of a minimal eIF4E-Cup complex reveals a general mechanism of eIF4E regulation in translational repression. *RNA* **18**, 1624-1634.

Kugler, J. and Lasko, P. (2009). Localization, anchoring and translational control of *oskar*, *gurken*, *bicoid* and *nanos* mRNA during *Drosophila* oogenesis. *Fly (Austin)* **3**, 15-28.

Lachance, P. E. D., Miron, M., Raught, B., Sonenberg, N. and Lasko, P. (2002). Phosphorylation of eukaryotic translation initiation factor 4E is critical for growth. *Mol. Cell. Biol.* **22**, 1656-1663.

Lin, A.C. and Holt, C.E. (2007). Local translation and directional steering in axons. *EMBO J.* **26**, 3729-3736.

Lindsley, D.T and Tokuyasu, K.T. (1980). Normal spermatogenesis in *Drosophila* (New York: Academic Press).

Macara, I.G., Iioka, H. and Mili, S. (2009). Axon growth-stimulus package includes local translation. *Nat. Cell Biol*. **11**, 919-921.

Mingle, L.A., Okuhama, N.N., Shi, J., Singer, R.H., Condeelis, J. and Liu, G. (2005). Localization of all seven messenger RNAs for the actin-polymerization nucleator Arp2/3 complex in the protrusions of fibroblasts. *J. Cell Sci.* **118**, 2425-2433.

Miron, M., Verdú, J., Lachance, P.E., Birnbaum, M.J., Lasko, P.F. and Sonenberg, N. (2001). The translational inhibitor 4E-BP is an effector of PI(3)K/Akt signalling and cell growth in *Drosophila*. *Nat. Cell Biol.* **3**, 596-601.

Moor, A.E., Golan, M., Massasa, E.E., Lemze, D., Weizman, T., Shenhav, R., Baydatch, S., Mizrahi, O., Winkler, R., Golani, O., Stern-Ginossar, N. and Itzkovitz, S. (2017). Global mRNA polarization regulates translation efficiency in the intestinal epithelium. *Science* **357**, 1299-1303.

Muro, I., Berry, D.L., Huh, J.R., Chen, C.H., Huang, H., Yoo, S.J., Guo, M., Baehrecke, E.H. and Hay, B.A. (2006). The *Drosophila* caspase Ice is important for many apoptotic cell deaths and for spermatid individualization, a nonapoptotic process. *Development* **133**, 3305-3315.

Nelson, M.R., Leidal, A.M. and Smibert, C.A. (2004). *Drosophila* Cup is an eIF4E-binding protein that functions in Smaug-mediated translational repression. *EMBO J.* **23**, 150-159.

Pelletier, J. and Sonenberg, N. (2019). The organizing principles of eukaryotic ribosome recruitment. *Annu. Rev. Biochem.* **88**, 307-335.

Perkins, L.A., Holderbaum, L., Tao, R., Hu, Y., Sopko, R., McCall, K., Yang-Zhou, D., Flockhart, I., Binari, R., Shim, H.S., et al. (2015). The transgenic RNAi project at Harvard Medical School: resources and validation. *Genetics* **201**, 843-852.

Peter, D., Igreja, C., Weber, R., Wohlbold, L., Weiler, C., Ebertsch, L., Weichenrieder, O. and Izaurralde, E. (2015). Molecular architecture of 4E-BP translation inhibitors bound to eIF4E. *Mol. Cell* **57**, 1074-1087.

Rathke, C., Baarends, W.M., Jayaramaiah-Raja, S., Bartkuhn, M., Renkawitz, R. and Renkawitz-Pohl, R. (2007). Transition from a nucleosome-based to a protamine-based chromatin configuration during spermiogenesis in *Drosophila*. *J. Cell Sci.* **120**, 1689-1700.

Raz, A. A., Vida, G. S., Stern, S. S., Mahadevaraju, S., Fingerhut, J. M., Viveiros, J. M., Pal, S., Grey, J. R., Grace, M. R., Berry, C. W., et al. (2022). Emergent dynamics of adult stem cell linages from single nucleus and single cell RNA-Seq of *Drosophila* testes. *BioRxiv* doi: 10.1101/2022.07.26.501581.

Rengan, A.K., Agarwal, A., van der Linde, M. and du Plessis, S.S. (2012). An investigation of excess residual cytoplasm in human spermatozoa and its distinction from the cytoplasmic droplet. *Reprod Biol Endocrinol* 10:92.

Renkawitz-Pohl, R., Hempel, L., Hollmann, M. and Schäfer, M.A. (2005). Spermatogenesis. In *Comprehensive Insect Physiology, Biochemistry, Pharmacology and Molecular Biology* (ed. L.I. Gilbert, K. Iatrou, S. Gill), pp. 157-78. Oxford: Elsevier.

Russica, V., Bawankar, P., Peter, D., Helms, S., Igreja, C. and Izaurralde, E. (2019). Direct role for the *Drosophila* GIGYF protein in 4EHP-mediated mRNA repression. *Nucleic Acids Res.* **17**, 7035-7048.

Santel, A., Winhauer, T., Blümer, N. and Renkawitz-Pohl, R. (1997). The Drosophila *don juan* (*dj*) gene encodes a novel sperm specific protein component characterized by an unusual domain of a repetitive amino acid motif. *Mech. Dev.* **64**, 19-30.

Schäfer, M., Börsch, D., Hülster, A. and Schäfer, U. (1993). Expression of a gene duplication encoding conserved sperm tail protein is translationally regulated in *Drosophila melanogaster*. *Mol. Cell. Biol.* **13**, 1708-1718.

Shaha, C., Tripathi, R. and Mishra, D.P. (2010). Male germ cell apoptosis: regulation and biology. *Philos. Trans. R. Soc. Lond. B Biol. Sci.* **365**, 1501-1515.

Shao, L. (2019). Investigating the roles and regulation of testis-specific eIF4Es during *Drosophila* spermatogenesis. *MSc thesis*, University of Toronto, Toronto, Canada.

Sonenberg, N. and Hinnebusch, A.G. (2009). Regulation of translation initiation in eukaryotes: mechanisms and biological targets. *Cell* **136**, 731-745.

Song, A., Labella, S., Korneeva, N.L., Keiper, B.D., Aamodt, E.J., Zetka, M. and Rhoads, R.E. (2010). A *C. elegans* eIF4E-family member upregulates translation at elevated temperatures of mRNAs encoding MSH-5 and other meiotic crossover proteins. *J. Cell Sci.* **123**, 2228-2237.

Valzania, L., Ono, H., Ignesti, M., Cavaliere, V., Bernardi, F., Gamberi, C., Lasko, P. and Gargiulo, G. (2016) *Drosophila* 4EHP is essential for the larval-pupal transition and required in the prothoracic gland for ecdysone biosynthesis. *Dev. Biol.* **410**, 14-23.

Vibranovski, M.D., Chalopin, D.S., Lopes, H.F., Long, M. and Karr, T.L. (2010). Direct evidence for postmeiotic transcription during *Drosophila melanogaster* spermatogenesis. *Genetics* **186**, 431-433.

Vibranovski, M.D., Lopes, H.F., Karr, T.L. and Long, M. (2009). Stage-specific expression profiling of *Drosophila* spermatogenesis suggests that meiotic sex chromosome inactivation drives genomic relocation of testis-expressed genes. *PLoS Genet.* **5**, e1000731.

Wiebe, S., Meng, X.Q., Kim, S.H., Zhang, X., Lacaille, J.C., Aguilar-Valles, A. and Sonenberg, N. (2020). The eIF4E homolog 4EHP (eIF4E2) regulates hippocampal long-term depression and impacts social behavior. *Mol. Autism* **11**, 92.

White-Cooper, H. (2010). Molecular mechanisms of gene regulation during *Drosophila* spermatogenesis. *Reproduction* **139**, 11-21.

White-Cooper, H. and Caporilli, S. (2013). Transcription and post-transcriptional regulation of *Drosophila* germline stem cells and their differentiating progeny. In *Transcriptional and Translational Regulation of Stem Cells* (ed. G. Hime and H. Abud), pp. 47-61. Dordrecht: Springer.

Xu, S., Hafer, N., Agunwamba, B. and Schedl, P. (2012). The CPEB protein Orb2 has multiple functions during spermatogenesis in *Drosophila melanogaster*. *PLoS Genet.* **8**, e1003079.

Xu, S., Tyagi, S. and Schedl, P. (2014). Spermatid cyst polarization in *Drosophila* depends upon apkc and the CPEB family translational regulator orb2. *PLoS Genet.* **10**, e1004380.

Zaccai, M. and Lipshitz, H.D. (1996). Role of *Adducin-like* (*hu-li tai shao*) mRNA and protein localization in regulating cytoskeletal structure and function during *Drosophila* oogenesis and early embryogenesis. *Dev. Genet.* **19**, 249-257.

Zappavigna, V., Piccioni, F., Villaescusa, J.C. and Verrotti, A.C. (2004). Cup is a nucleocytoplamic shuttling protein that interacts with the eukaryotic translation initiation factor 4E to modulate *Drosophila* ovary development. *Proc. Natl. Acad. Sci. USA* **101**, 14800-14805.

Zhao, J., Klyne, G., Benson, E., Gudmannsdottir, E., White-Cooper, H. and Shotton, D. (2010). FlyTed: the *Drosophila* testis gene expression database. *Nucleic Acids Res.* **38**, D710-715.

Zhou, X., Fabian, L., Bayraktar, J.L., Ding, H-M., Brill, J.A. and Chang, H.C. (2011). Auxilin is required for formation of Golgi-derived clathrin-coated vesicles during *Drosophila* spermatogenesis. *Development* **138**, 1111-1120.

Zuberek, J., Kuchta, K., Hernández, G., Sonenberg, N. and Ginalski, K. (2016). Diverse cap-binding properties of *Drosophila* eIF4E isoforms. *Biochim. Biophys. Acta* **1864**, 1292-1303.

Figures

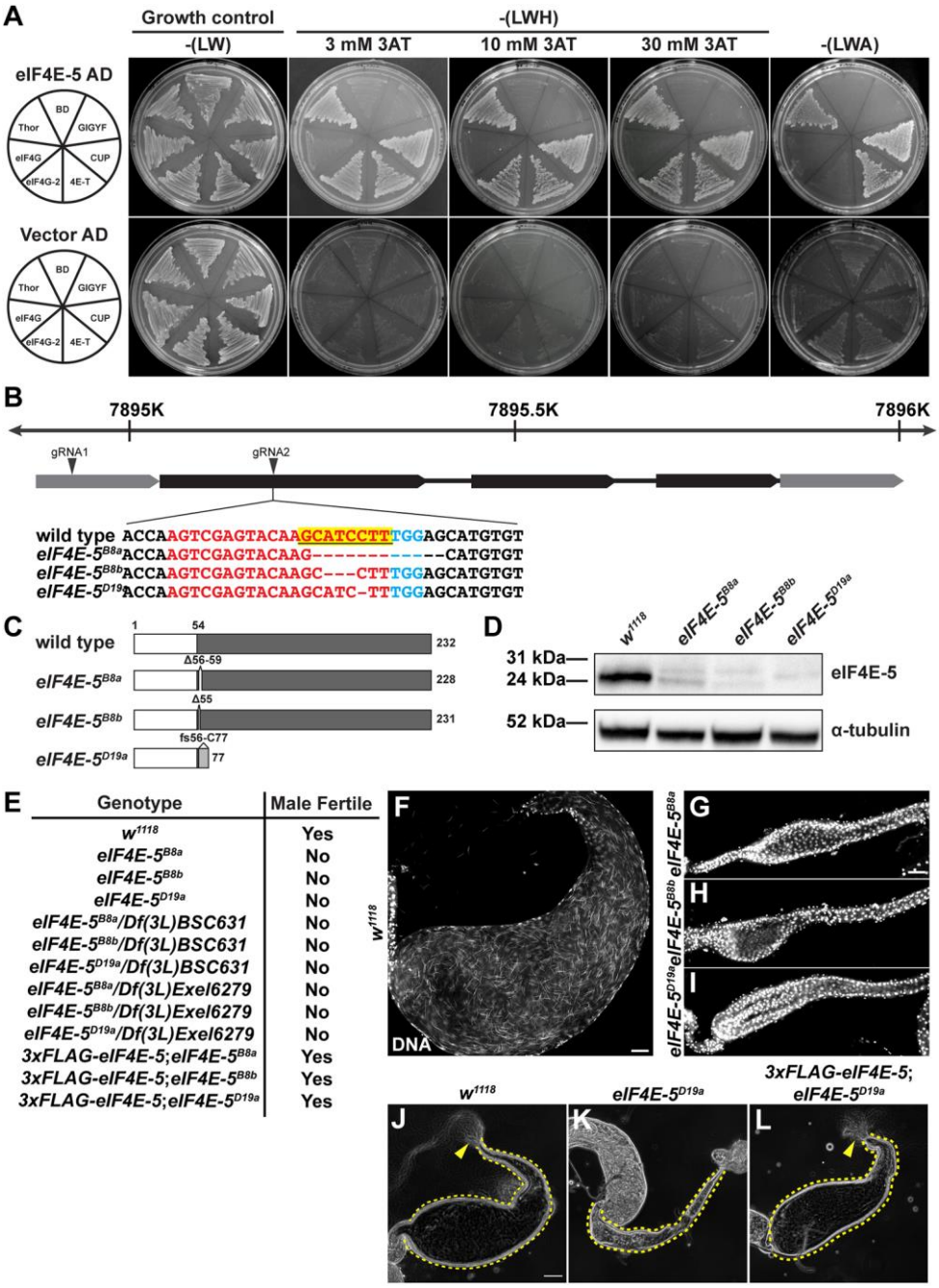

Fig. 1. eIF4E-5 interacts with known translation regulators and is required for male fertility. (A) eIF4E-5 interacts with Cup, 4E-T, eIF4G-2, and Thor in yeast two-hybrid assays, as revealed by growth on selective medium, whereas eIF4E-5 does not interact with eIF4G-2 or

GIGYF, as revealed by lack of growth on selective medium. pOBD2 (BD; empty GAL4 DNA binding domain vector) and pOAD (AD; empty activation domain vector) were used as negative controls. L, leucine; W, tryptophan; H, histidine; A, adenine; 3AT, 3-amino-1,2,4-triazole. Data are representative of three independent experiments. **(B)** CRISPR/Cas9 mutagenesis was used to generate mutants of *eIF4E-5*. Diagram showing nucleotide position of *eIF4E-5* on chromosome 3L (top). Gene structure: 5' and 3' UTRs (grey boxes), coding exons (black boxes), introns (lines). Locations of gRNAs in 5'UTR (gRNA1) and first exon (gRNA2) are indicated. *eIF4E-5*^{B8a}, *eIF4E-5*^{B8b} and *eIF4E-5*^{D19a} mutants contain deletions in the first exon, overlapping gRNA2. Genomic sequence: protospacer adjacent motif (blue), target region of the gRNA (red), deletions (dashed lines), conserved eIF4G or 4E-BP binding motif of His55, Pro56, Leu57 (underlined yellow highlight). **(C)** Structure of predicted wild-type (top) and mutant eIF4E-5 proteins. eIF4E-5 has a non-conserved N-terminus (amino acids 1-53; white box) and conserved C-terminus (amino acids 54-232; dark grey box). In-frame deletions encoded by *eIF4E-5*^{B8a} and *eIF4E-5*^{B8b} and frameshift (fs) mutation encoded by *eIF4E-5*^{D19a} (out-of-frame amino acids 56-77; light grey box) are indicated. **(D)** Immunoblot of total testis extracts probed with the indicated antibodies reveals reduced (*eIF4E-5*^{B8a}, *eIF4E-5*^{B8b}) or undetectable (*eIF4E-5*^{D19}) levels of eIF4E-5 protein. Note that these levels correlate with the severity of the phenotypes shown in Figs 2, 3 and 5. α-tubulin was used as the loading control. Blot is representative of three independent experiments (40 testes dissected per genotype). **(E)** Fertility tests reveal that all tested combinations of *eIF4E-5* alleles and deficiencies are male sterile and that a genomic transgene expressing 3xFLAG-eIF4E-5 restores fertility to *eIF4E-5*^{B8a}, *eIF4E-5*^{B8b} and *eIF4E-5*^{D19a} homozygous mutant males. Number of males tested per genotype (top to bottom): 17, 16, 23, 18, 10, 10, 10, 10, 10, 10, 14, 13, 17. **(F-I)** Laser-scanning confocal fluorescence micrographs demonstrate presence of needle-shaped sperm nuclei in control (E) but not *eIF4E-5*^{B8a} (G), *eIF4E-5*^{B8b} (H) or *eIF4E-5*^{D19a} (I) seminal vesicles stained with DAPI. Number of seminal vesicles examined per genotype (left to right, top to bottom): 8, 5, 5, 6. Scale bars: 20 µm. **(J-L)** Phase-contrast micrographs of live 7-day old control (J), *eIF4E-5*^{D19a} (K), or *3xFLAG-eIF4E-5;eIF4E-5*^{D19a} (L) seminal vesicles reveal presence of mature, motile sperm (yellow arrowheads) in mutants carrying 3xFLAG-eIF4E-5 transgene. Number of seminal vesicles examined per genotype (left to right): 14, 10, 12. Scale bar: 50 µm.

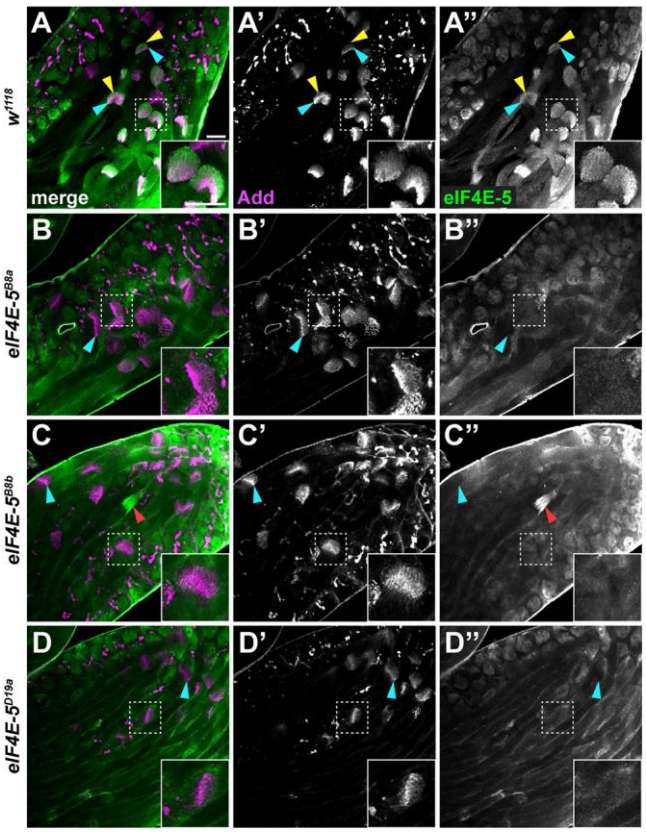

Fig. 2. eIF4E-5 localizes to the distal ends of elongated spermatid cysts. (A-D) Laser-scanning confocal fluorescence micrographs of control (A), *eIF4E-5*^{B8a} (B), *eIF4E-5*^{B8b} (C) or *eIF4E-5*^{D19a} (D) whole adult testes stained for Adducin (Add; magenta, cyan arrowheads) and eIF4E-5 (green, yellow arrowheads) reveals that eIF4E-5 localizes just distal to Adducin at the ends of elongated spermatid cysts in control but not *eIF4E-5* mutant spermatid cysts. Note that anti-eIF4E-5 antibodies non-specifically stain individualization complexes, as shown for the mispolarized cyst in *eIF4E-5*^{B8b} (C-C'', red arrowheads). Images are representative of at least two sets of experiments (10 testes dissected per genotype). Scale bars: 20 µm.

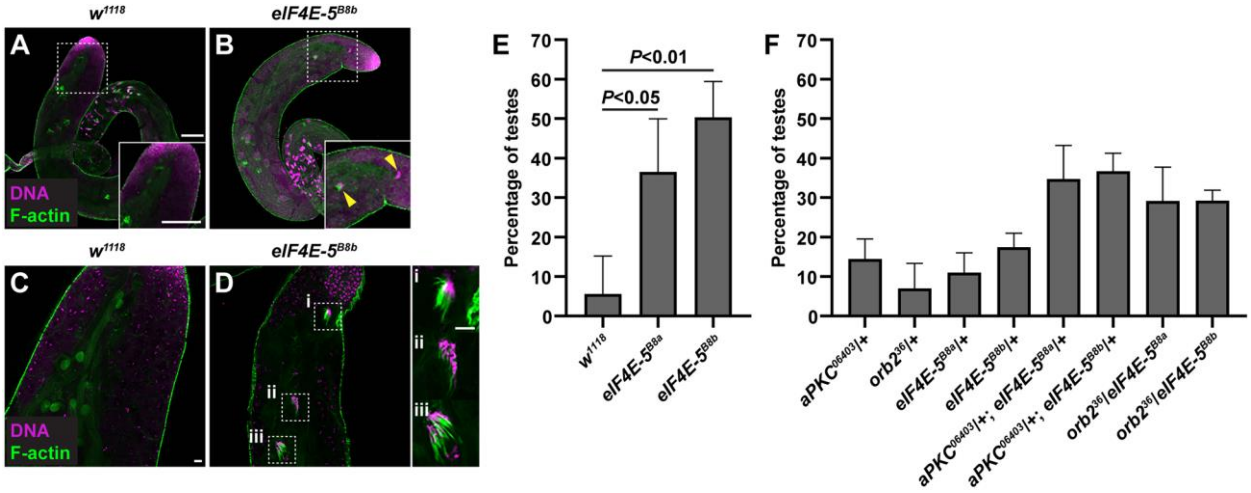

Fig. 3. eIF4E-5 acts with Orb2 and aPKC to regulate spermatid cyst polarity. (A-D) Laser-scanning confocal fluorescence micrographs of control (A, C) or *eIF4E-5*^{B8b} (B, D) whole adult testes stained for DNA (magenta) and F-actin (green). Nuclei in elongated spermatid cysts orient towards the basal end in control testes, whereas occasional clusters of nuclei orient towards the testis tip in *eIF4E-5*^{B8b} mutants (B, D; quantified in E). Scale bars: 100 µm. **(E-F)** Percentage of testes with at least one cluster of spermatid nuclei found at the apical tip instead of the basal end of the testes. Error bars: standard deviation based on three sets of experiments. Student *t*-tests were unpaired. (E) Percentage of testes with misoriented spermatid cysts was significantly higher in homozygous *eIF4E-5* mutants compared to control: *eIF4E-5*^{B8a} (P<0.05) and *eIF4E-5*^{B8b} (P<0.01). Number of testes scored for each genotype (left to right): 17, 32, 25. (F) Percentage of testes with misoriented spermatid cysts was significantly higher in each of the transheterozygotes relative to their respective heterozygous controls: *aPKC*^{06403}/+; *eIF4E-5*^{B8a}/+ and *aPKC*^{06403}/+ (P<0.05) and *eIF4E-5*^{B8a}/+ (P<0.05), *aPKC*^{06403}/+; *eIF4E-5*^{B8b}/+ and *aPKC*^{06403}/+ (P<0.01) and *eIF4E-5*^{B8b}/+ (P<0.01), *orb2*^{36}/*eIF4E-5*^{B8a} and *orb2*^{36}/+ (P<0.05) and *eIF4E-5*^{B8a}/+ (P<0.05), *orb2*^{36}/*eIF4E-5*^{B8b} and *orb2*^{36}/+ (P<0.01) and *eIF4E-5*^{B8b}/+ (P=0.01). Number of testes scored for each genotype (left to right): 30, 28, 31, 72, 145, 108, 125.

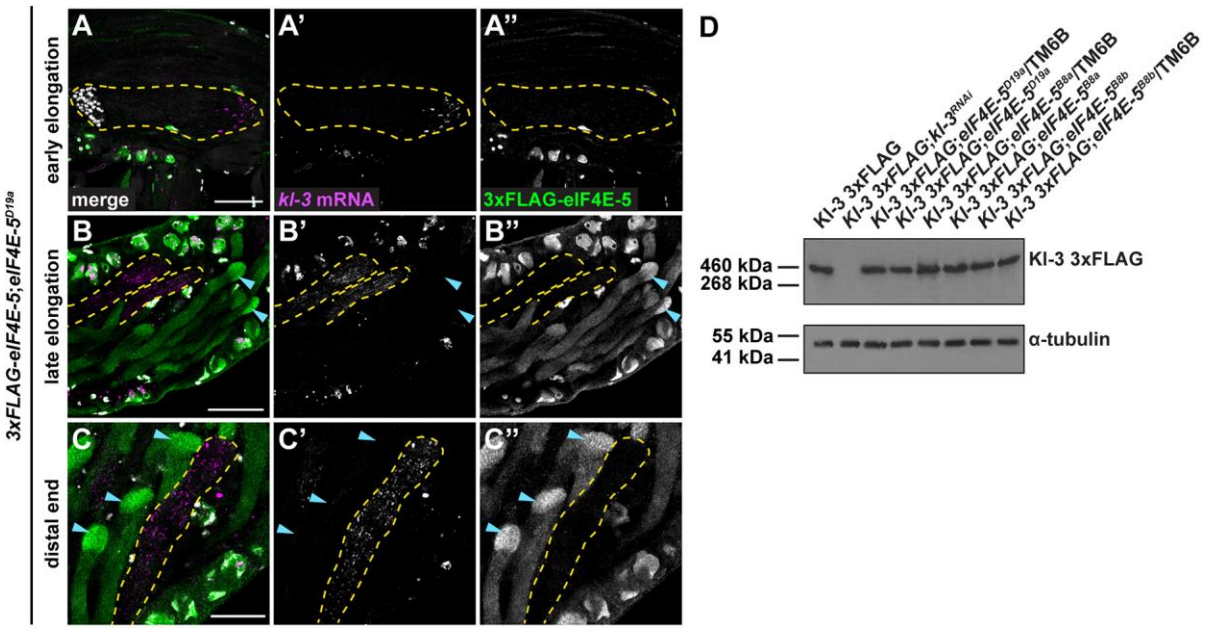

Fig. 4. Accumulation of axonemal dynein Kl-3 is independent of *eIF4E-5*. (A-C) Laser-scanning confocal fluorescence micrographs of *3xFLAG-eIF4E-5;eIF4E-5*^{D19a} whole adult testes probed for *kl-3* mRNA (magenta) and stained for 3xFLAG-eIF4E-5 protein (green) and DNA (white). *kl-3* mRNA (cysts outlined by dotted yellow lines) does not colocalize with eIF4E-5 protein (cyan arrowheads) at the distal ends of early or late elongating spermatid cysts. Images are representative of two independent experiments (40 testes dissected per repeat). Scale bars: 50 µm. **(D)** Immunoblot of whole testis extracts reveals that endogenously tagged Kl-3 3xFLAG protein levels are unaffected in *eIF4E-5* mutants. α-tubulin was used as the loading control. Blot is representative of three independent experiments (80 testes dissected per genotype).

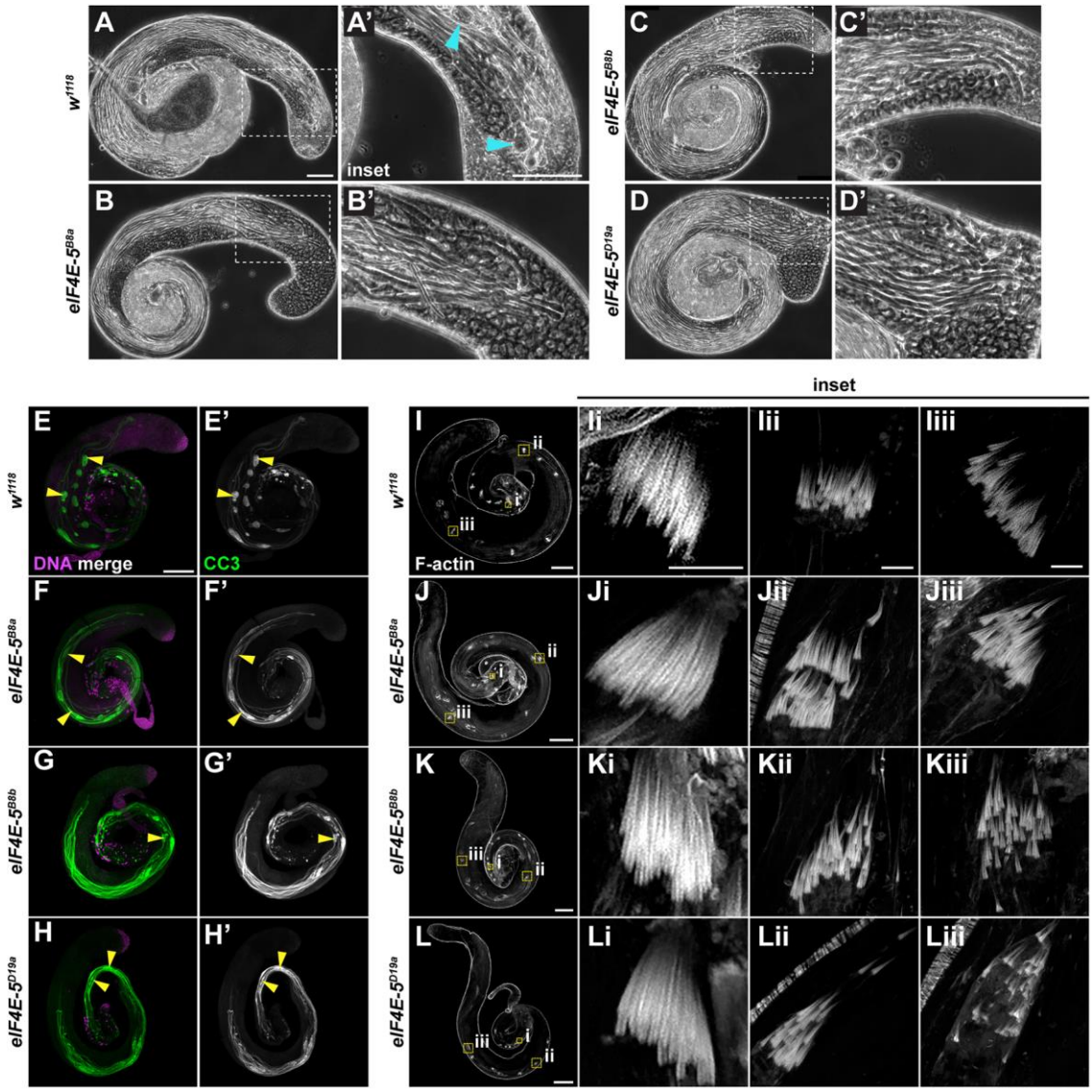

Fig. 5. *eIF4E-5* mutants exhibit defects in individualization. (A-D) Phase-contrast images of 4-day old control (A), *eIF4E-5*^{B8a} (B), *eIF4E-5*^{B8b} (C) or *eIF4E-5*^{D19a} (D) testes reveal an absence of waste bags (cyan arrowheads) near the apical testis tip in *eIF4E-5* mutants. Number of testes examined per genotype (top to bottom, left to right): 11, 10, 16, 13. Scale bar: 100 µm. **(E-H)** Laser-scanning confocal fluorescence micrographs of control (E), *eIF4E-5*^{B8a} (F), *eIF4E-5*^{B8b} (G) or *eIF4E-5*^{D19a} (H) whole adult testes stained for DNA (magenta) and activated (cleaved) caspase-3 (CC3; green). Activated caspase (yellow arrowheads) is restricted to cystic bulges in control (E) but not *eIF4E-5* mutants (F-H). Images are representative of at least two sets of experiments (10 testes dissected per genotype). Scale bar: 200 µm. **(I-L)** Laser-scanning

confocal fluorescence micrographs of control (I), *eIF4E-5*^{B8a} (J), *eIF4E-5*^{B8b} (K) or *eIF4E-5*^{D19a} (L) whole adult testes stained for F-actin (white). Boxed areas are magnified 4 or 5-fold in insets. Groups of actin cones in individualization complexes move synchronously down the length of cysts in control (Ii-Iiii) but become scattered prior to reaching the distal end of elongated spermatid cysts in *eIF4E-5* mutants (Ji-Liii). Images are representative of three sets of experiments (10 testes dissected per genotype). Scale bars: 100 µm (whole tissue), 10 µm (insets).

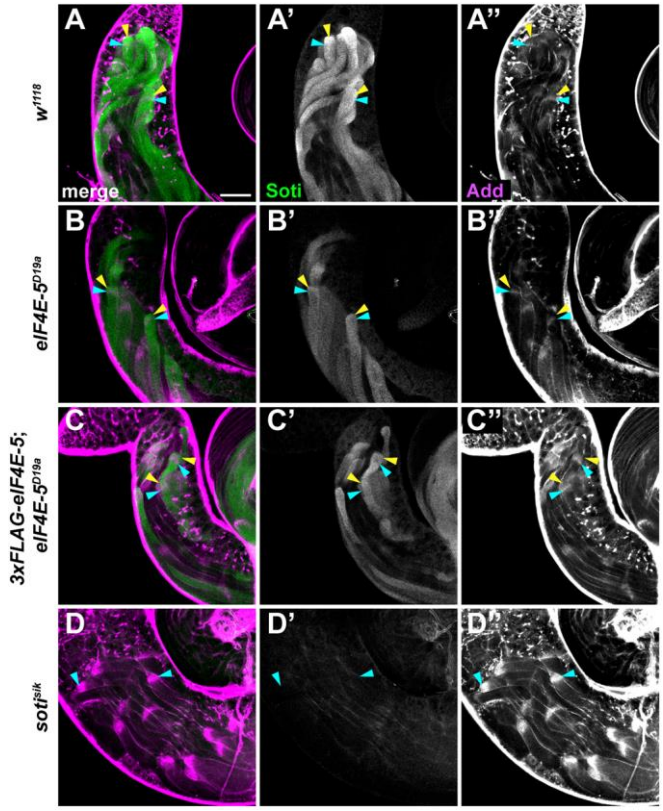

Fig. 6. eIF4E-5 is required for localized accumulation of Soti, a caspase inhibitor. (A-D) Laser-scanning confocal fluorescence micrographs of control (A), *eIF4E-5*^{D19a} (B) *3xFLAG-eIF4E-5;eIF4E-5*^{D19a} rescue (C) or *soti*^{sik} (D) whole adult testes stained for Adducin (Add; magenta, cyan arrowheads) and Soti (green). Soti is enriched at distal ends of elongated spermatid cysts in control, reduced in *eIF4E-5*^{D19a}, partially restored in rescue, and absent in *soti*^{sik} (yellow arrowheads). Images are representative of three sets of experiments (12 testes dissected per genotype). Scale bars: 50 µm.

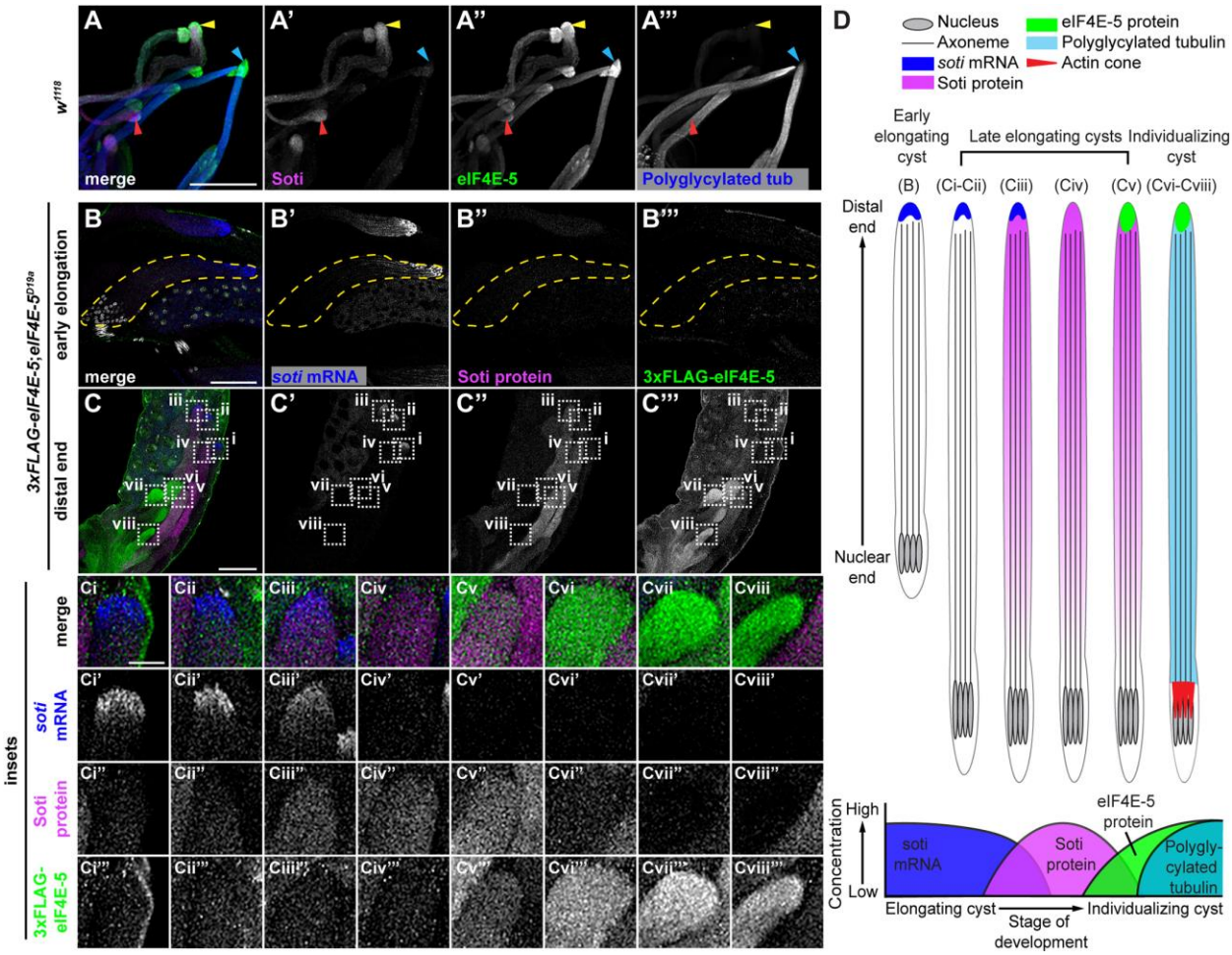

Fig. 7. eIF4E-5 colocalizes with Soti protein but not *soti* mRNA at the distal ends of elongated spermatid cysts. Laser-scanning confocal fluorescence micrographs. **(A)** Control whole adult testis stained for Soti (magenta), eIF4E-5 (green) and polyglycylated tubulin (blue). Soti colocalizes with eIF4E-5 (red arrowhead). eIF4E-5 becomes enriched at distal ends of elongated cysts as Soti levels decline prior to individualization (yellow arrowhead) and persists during individualization in cysts marked by polyglycylated tubulin (cyan arrowhead). Images are representative of two sets of experiments (10 testes dissected per repeat). Scale bar: 50 µm. **(B-C)** *3xFLAG-eIF4E-5;eIF4E-5*^{D19a} whole adult testes probed for *soti* mRNA (blue; cyst outline by dotted yellow line) and stained for Soti protein (magenta), 3xFLAG-eIF4E-5 protein (green) and DNA (white in B, C). Images reveal varying extents of *soti*, Soti and eIF4E-5 colocalization at the distal ends of elongated spermatid cysts. Boxed areas (C) are magnified 3-fold in insets.

Images are representatives of two sets of experiments (40 testes dissected per repeat). Scale bars: 50 µm (B-C) and 10 µm (Ci-Cviii). **(D)** Model for *soti* mRNA, Soti protein, eIF4E-5 protein and polyglycylated tubulin expression and localization during spermiogenesis. Note that elongating and individualizing cysts have 64 spermatids, but only four are shown for simplicity.

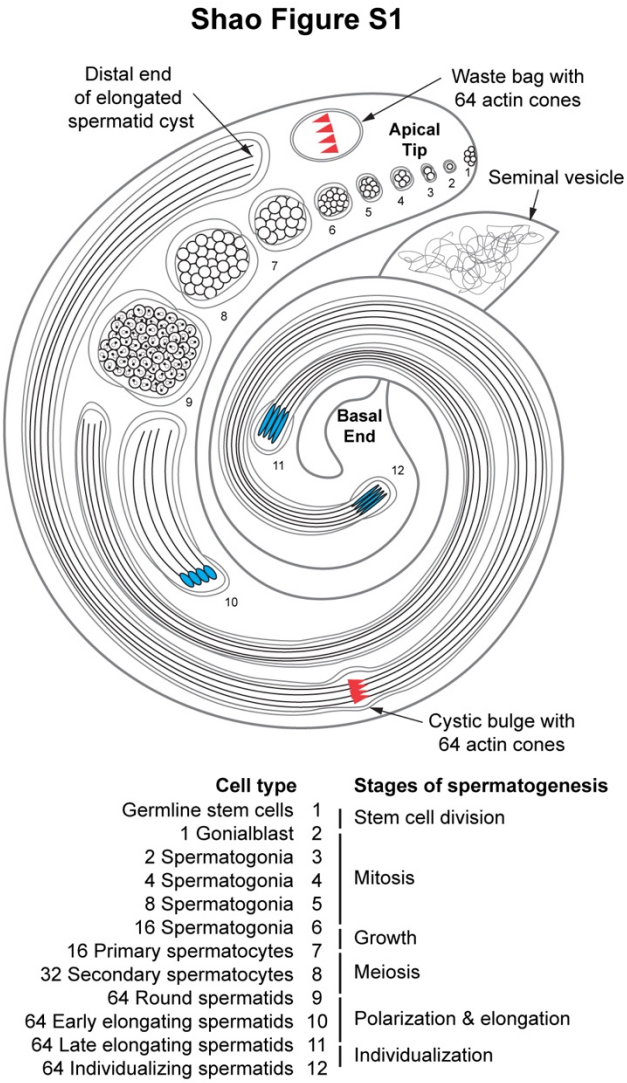

Fig. S1. Stages of spermatogenesis are organized in a spatiotemporal manner within the *Drosophila* testis. Whole adult testis and seminal vesicle showing stages of spermatogenesis described in the text. Developing germline cells are enclosed by somatic cyst cells throughout spermatogenesis. Note that spermatid cysts undergoing elongation and individualization (blue nuclei, red actin cones) have 64 spermatids, but only four are shown for simplicity.

Shao Figure S2

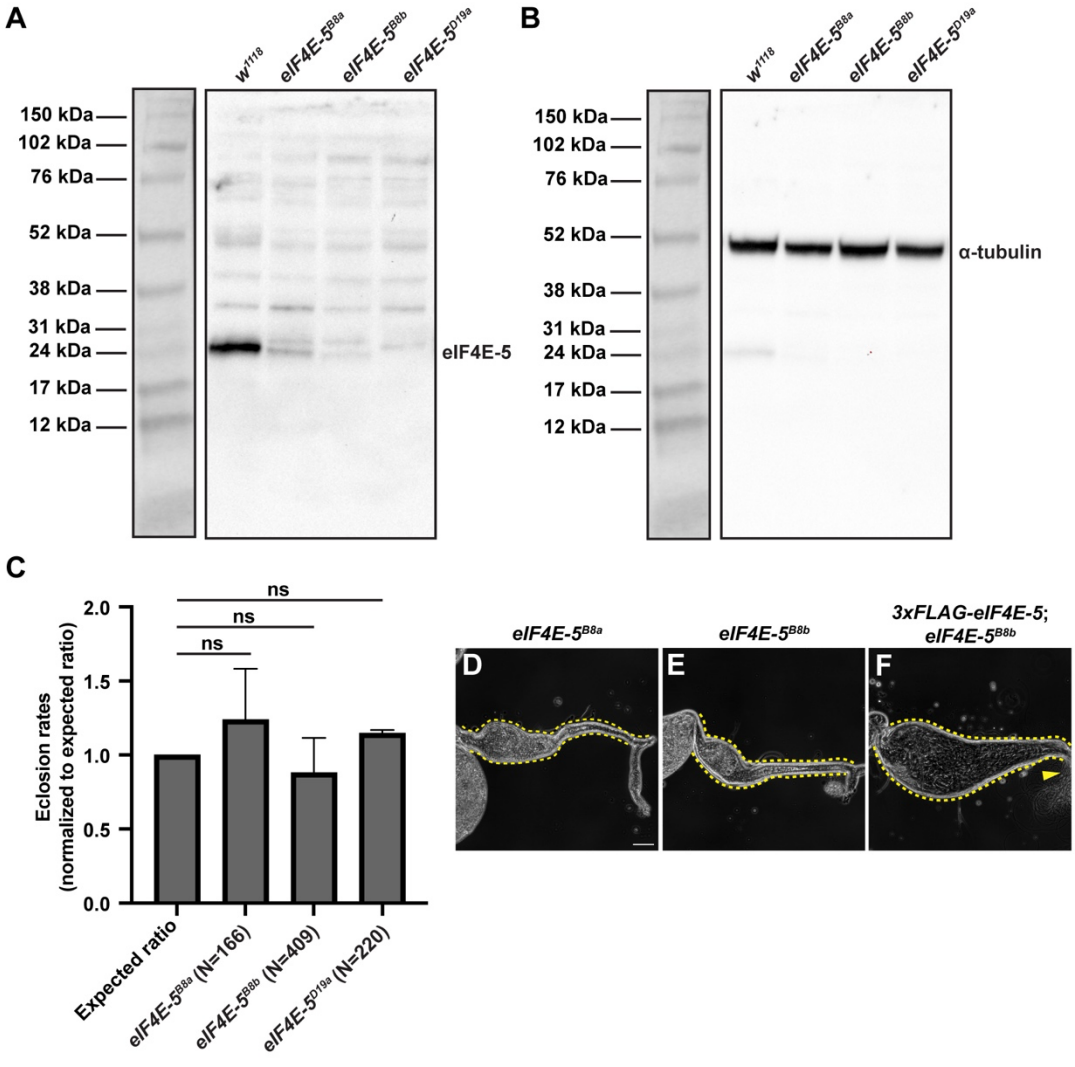

Fig. S2. *eIF4E-5* mutants affect eIF4E-5 protein levels but not viability and are rescued by expression of 3xFLAG-eIF4E-5. (A-B) Whole immunoblots of total testis extracts probed with anti-eIF4E-5 (A) or anti-α-tubulin (B) reveal reduced (*eIF4E-5^{B8a}* and *eIF4E-5^{B8b}*: predicted molecular weights ~26.4 kDa and ~26.8 kDa, respectively) or undetectable (*eIF4E-5^{D19}*: predicted molecular weight ~8.4 kDa) levels of eIF4E-5 protein. α-tubulin was used as the loading control. Blot is representative of three independent experiments (40 testes per genotype). **(C)** No significant difference was observed in eclosion rates of homozygous *eIF4E-5* mutants relative to the expected Mendelian ratio. Number of progeny scored for each genotype (left to right): 166, 409, 220. ns = not significant. Error bars: standard deviation based on two sets of experiments for *eIF4E-5^{B8a}* and *eIF4E-5^{D19a}*, and four sets for *eIF4E-5^{B8b}*. One way ANOVA with Dunnett's multiple comparison test was used. **(D-F)** Phase-contrast micrographs of 7-day old *eIF4E-5^{B8a}* (D), *eIF4E-5^{B8b}* (E), or *3xFLAG-eIF4E-5;eIF4E-5^{B8b}* (F) reveal presence of mature, motile sperm (yellow arrowheads) in seminal vesicles of mutants carrying 3xFLAG-eIF4E-5 transgene. Number of testes examined from left to right: 15, 14, and 11. Scale bar: 50 μm.

Shao Figure S3

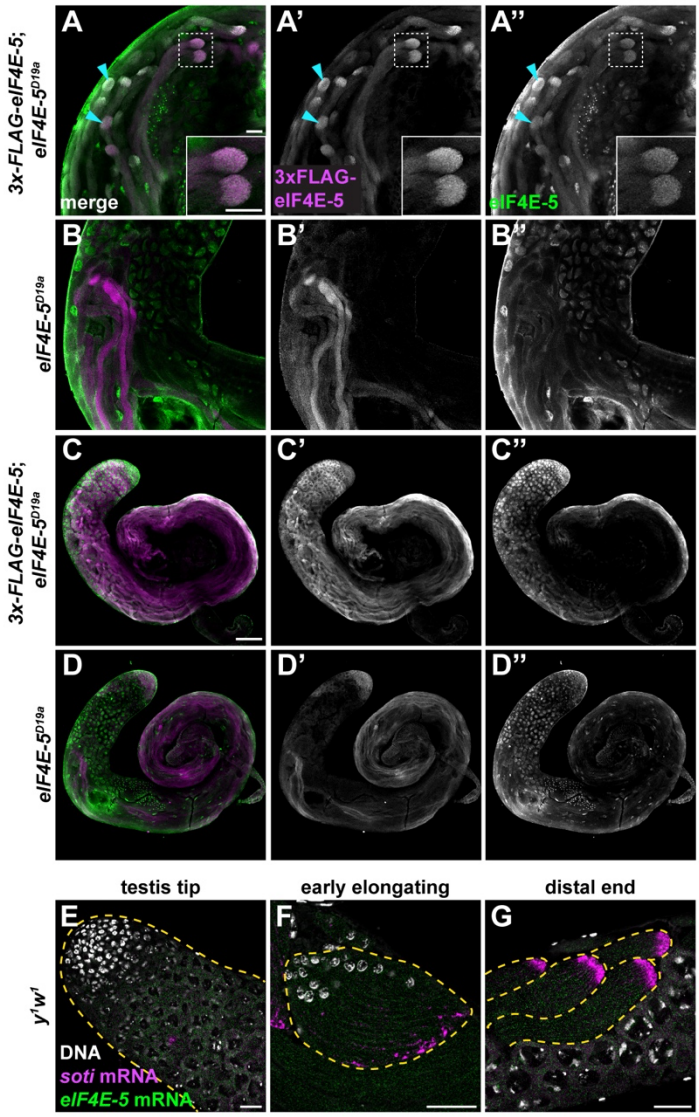

Fig. S3. 3xFLAG-eIF4E-5 localizes to the distal ends of elongated spermatid cysts. (A-D) Laser-scanning confocal fluorescence micrographs of *3x-FLAG-eIF4E-5*;*eIF4E-5*^{D19a} (A,C) or *eIF4E-5*^{D19a} (B,D) whole adult testes stained for 3xFLAG-eIF4E-5 (magenta) and endogenous eIF4E-5 (green). 3xFLAG-eIF4E-5 and eIF4E-5 colocalize at the distal end of elongated spermatid cysts (A; cyan arrowheads). Note non-specific staining of spermatogonia and spermatid tails with anti-FLAG antibodies and non-specific staining of nuclei in spermatogonia, spermatocytes and round spermatids with anti-eIF4E-5 antibodies (A-D'') in *eIF4E-5*^{D19a} mutants. Images are representative of two independent sets of experiments (10 testes dissected per genotype). Scale bars: 20 µm (A-B), 100 µm (C-D). **(E-G)** Whole adult testes of control probed for *soti* mRNA (magenta) and *eIF4E-5* mRNA (green) and stained for DNA (white). Distribution of *eIF4E-5* mRNA is diffuse during early and late stages of spermatogenesis. Images are representative of two independent experiments (30 testes per repeat). Scale bars: 25 µm.

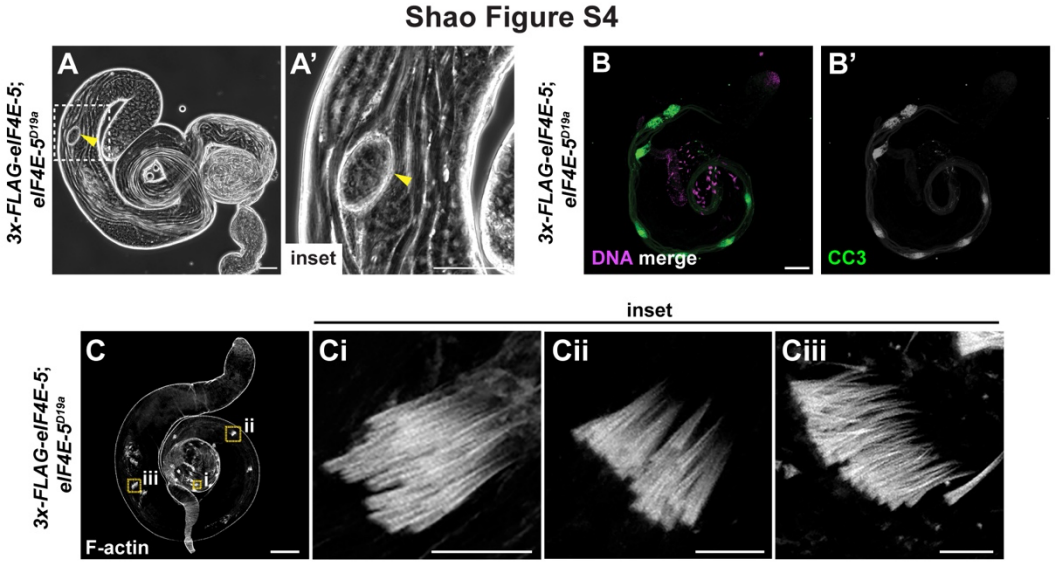

Fig. S4. Individualization is restored in *eIF4E-5* mutants expressing 3xFLAG-eIF4E-5. (A) Phase-contrast micrographs of 3-day old *3xFLAG-eIF4E-5;eIF4E-5^{D19a}* testis revealing presence of waste bag (yellow arrowheads). 13 testes were examined. Scale bars: 50 µm. **(B)** Laser-scanning confocal fluorescence micrographs of *3xFLAG-eIF4E-5;eIF4E-5^{D19a}* whole adult testis stained for DNA (magenta) and activated (cleaved) caspase-3 (CC3; green). Activated caspase is restricted to cystic bulges. Images are representative of two sets of experiments (10 testes dissected per repeat). Scale bar: 100 µm. **(C)** Laser-scanning confocal fluorescence micrograph of *3xFLAG-eIF4E-5;eIF4E-5^{D19a}* whole adult testis stained for F-actin (white). Boxed area is magnified 5-fold in insets. Groups of actin cones in individualization complex move synchronously down the length of the cysts. Images are representative of two sets of experiments (10 testes dissected per repeat). Scale bars: 100 µm (whole tissue), 10 µm (insets).

Shao Figure S5

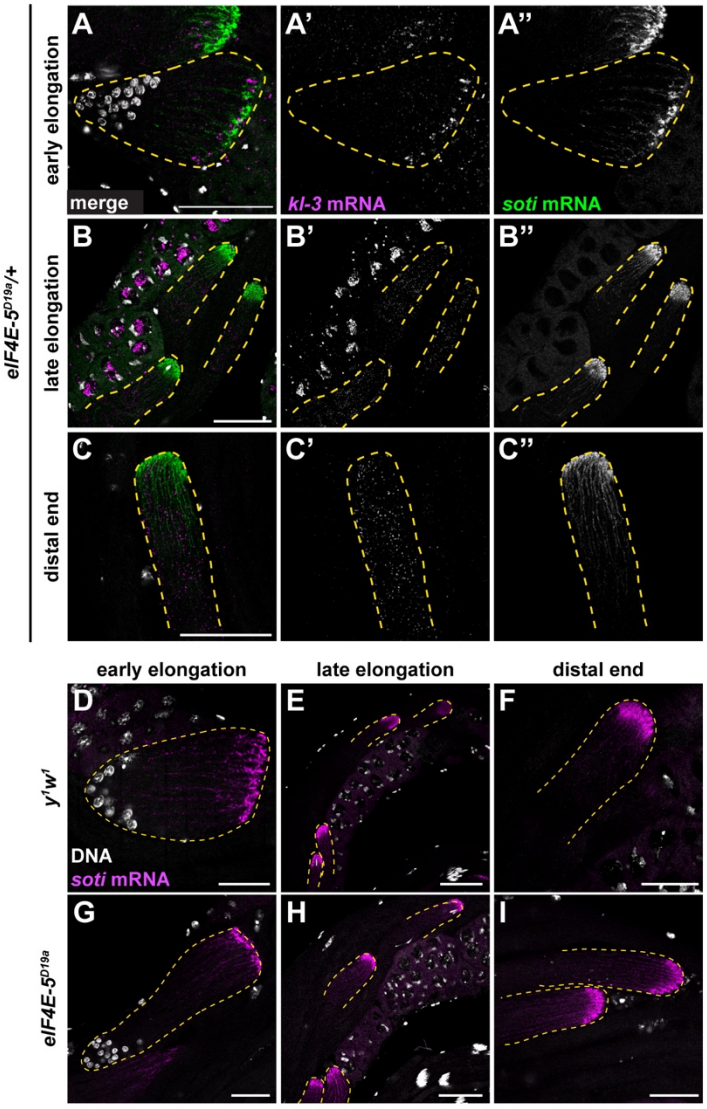

Fig. S5. *eIF4E-5* mRNA is diffusely present in male germ cells, and eIF4E-5 does not colocalize with *kl-3* mRNA and is not required for *soti* mRNA distribution. Laser-scanning confocal fluorescence micrographs. **(A-C)** Whole adult testes of control probed for *kl-3* mRNA (magenta) and *soti* mRNA (green) and stained for DNA (white). *kl-3* mRNA (cysts outlined by dotted yellow lines) does not colocalize with *soti* mRNA at the distal end of elongating spermatid cysts. Images are representative of two independent experiments (30 testes dissected per repeat). Scale bars: 50 µm. **(D-I)** Control (D-F) and *eIF4E-5*^{D19a} (G-I) whole adult testes probed for *soti* mRNA (magenta) and DNA (white). Levels and localization of *soti* mRNA at the distal ends of elongated cysts (cysts outlined by dotted yellow lines) appear similar in control and *eIF4E-5* mutants. Images are representative of two independent sets of experiments (30 testes dissected per genotype). Scale bars: 25 µm (D, G), 50 µm (E-F, H-I).

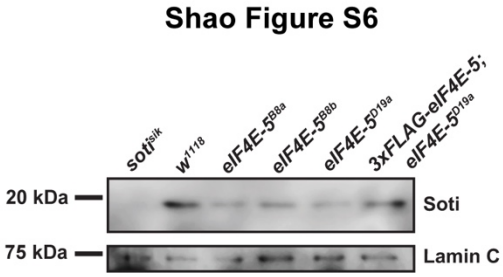

Fig. S6. Soti protein levels are reduced in *eIF4E-5* mutants. Immunoblot of whole testis extracts reveals reduced Soti levels in all three *eIF4E-5* mutants. Lamin C was used as the loading control. Blot represents a single experiment where all genotypes were included (40 testes dissected per genotype). Two other experiments showed a similar trend.

Table S1. Probes used for RNA FISH.

Click here to download Table S1